erg) (7.2)

To give some per-
round state is about
gy of about 13.6 eV.
will be measured in
he relation between

(7.3)

Using the physical

(7.4)

Part II

Scattering

8

Boundary Conditions

In many systems of interest, particles are incident on a target from some particular direction. For example, in a scattering experiment electrons might be beamed from an electron gun at a hydrogen target. Some of the electrons may propagate through the target, others may be reflected by the target. In this chapter we learn how to impose such physically realistic boundary conditions on one-dimensional problems.

We begin by representing the target by a stationary one-dimensional potential with asymptotic values V_L, V_R on the left and right. The particle incident from the left is represented by the wavefunction $A_L e^{+ik_L x}, k_L = [2m(E - V_L)/\hbar^2]^{1/2}$. The wavefunction representing the reflected particle is $B_L e^{-ik_L x}$; the wavefunction representing the transmitted particle is $A_R e^{+ik_R x}$. Thus, the boundary condition for a particle incident on the target from the left is $B_R = 0$.

We have seen in chapter 5 that the law of momentum conservation can be written as

$$\hbar k_L(|A_L|^2 - |B_L|^2) = \hbar k_R(|A_R|^2 - |B_R|^2)\,. \tag{8.1}$$

For a particle incident from the left ($B_R = 0$), this expression can be written

$$\left|\frac{B_L}{A_L}\right|^2 + \frac{k_R}{k_L}\left|\frac{A_R}{A_L}\right|^2 = 1\,. \tag{8.2}$$

Since B_L is the probability amplitude for the reflected particle and A_L is the probability amplitude for the incident particle, $|B_L/A_L|^2$ has a natural interpretation as the probability that the incident particle is reflected. If the particle is not reflected or absorbed, it is transmitted. Therefore, $(k_R/k_L)|A_R/A_L|^2$ must be interpreted as

the probability that the incident particle is transmitted. In summary, the transmission (T) and reflection (R) probabilities are

$$T = \frac{k_R}{k_L}\left|\frac{A_R}{A_L}\right|^2 , \qquad R = \left|\frac{B_L}{A_L}\right|^2 , \qquad T + R = 1 . \tag{8.3}$$

Since

$$\begin{bmatrix} A_L \\ B_L \end{bmatrix} = \begin{bmatrix} t_{11}(E) & t_{12}(E) \\ t_{21}(E) & t_{22}(E) \end{bmatrix} \begin{bmatrix} A_R \\ B_R = 0 \end{bmatrix} = \begin{bmatrix} t_{11}(E)A_R \\ t_{21}(E)A_R \end{bmatrix} , \tag{8.4}$$

it follows that

$$T = \frac{k_R}{k_L}\left|\frac{1}{t_{11}(E)}\right|^2 . \tag{8.5}$$

This condition can be made more explicit by expressing $T(E)$ in terms of the product of matrices $M(V_j;\delta_j)$ for the interior pieces of the potential, and the pair of matrices for the two asymptotic regions

$$\begin{bmatrix} A \\ B \end{bmatrix}_L = \begin{bmatrix} e^{+ik_L a_L} & 0 \\ 0 & e^{-ik_L a_L} \end{bmatrix}^{-1} \begin{bmatrix} 1 & 1 \\ +ik_L & -ik_L \end{bmatrix}^{-1} \prod_{j=1}^{N} M(V_j;\delta_j)$$
$$\times \begin{bmatrix} 1 & 1 \\ +ik_R & -ik_R \end{bmatrix} \begin{bmatrix} e^{+ik_R a_R} & 0 \\ 0 & e^{-ik_R a_R} \end{bmatrix} \begin{bmatrix} A \\ B \end{bmatrix}_R . \tag{8.6}$$

It is convenient to absorb the exponentials into the definition of the amplitudes. Carrying out the remaining matrix multiplications, we obtain

$$\begin{bmatrix} A \\ B \end{bmatrix}_L' = \begin{bmatrix} \alpha_R + i\alpha_I & \beta_R + i\beta_I \\ \beta_R - i\beta_I & \alpha_R - i\alpha_I \end{bmatrix} \begin{bmatrix} A \\ B \end{bmatrix}_R' , \tag{8.7}$$

$$2\alpha_R = +m_{11} + \frac{k_R}{k_L}m_{22} , \qquad 2\alpha_I = +k_R m_{12} - \frac{m_{21}}{k_L} ,$$

$$2\beta_R = +m_{11} - \frac{k_R}{k_L}m_{22} , \qquad 2\beta_I = -k_R m_{12} - \frac{m_{21}}{k_L} ,$$

where $A_L' = A_L e^{+ik_L a_L}$ and so on, and a_L, a_R are the left- and right-hand boundaries of the potential. Then $|A_L'|^2 = |A_L|^2$ and so on, so that $T(E) = (k_R/k_L)|A_R'/A_L'|^2$. As a result, the transmission probability is given by

$$T(E) = \frac{4(k_R/k_L)}{\left[m_{11} + (k_R/k_L)m_{22}\right]^2 + \left[k_R m_{12} - m_{21}/k_L\right]^2} . \tag{8.8}$$

In the typically encountered case in which $V_L = V_R$, $k_L = k_R = k$ and this expression simplifies to

$$T(E) = \frac{4}{\left(m_{11} + m_{22}\right)^2 + \left(k m_{12} - m_{21}/k\right)^2} . \tag{8.9}$$

This is the expression we use to compute almost all transmission probabilities in this work.

To illustrate
barrier with
$V_L = V_R$
$\sqrt{2mE/\hbar^2}$
$m_{ij}(E)$ for
4.1. There a

$E < V$:

$E = V$:

9

A Simple Example

To illustrate these results, we compute the transmission probability for the rectangular barrier with constant potential V, width δ, shown in the inset of Fig. 9.1. We assume $V_L = V_R = 0$. The transfer matrix is given by (4.12). Since $k_L = k_R = k = \sqrt{2mE/\hbar^2}$, the transmission probability is $T = |1/t_{11}(E)|^2$. The matrix elements $m_{ij}(E)$ for the single intermediate potential can be seen by inspection from Table 4.1. There are three cases to consider:

$E < V$: $\kappa = \sqrt{2m(V-E)/\hbar^2}$,

$$t_{11}(E) = \cosh\kappa\delta - \frac{i}{2}\left(-\frac{\kappa}{k}+\frac{k}{\kappa}\right)\sinh\kappa\delta\,, \tag{9.1}$$

$$T(E) = \frac{1}{\cosh^2\kappa\delta + \frac{1}{4}\left(\frac{\kappa}{k}-\frac{k}{\kappa}\right)^2\sinh^2\kappa\delta} = \frac{1}{1+\frac{1}{4}\left(\frac{\kappa}{k}+\frac{k}{\kappa}\right)^2\sinh^2\kappa\delta}\,; \tag{9.2}$$

$E = V$:

$$t_{11}(E) = 1 - ik\delta/2\,, \tag{9.3}$$

$$T(E) = \frac{1}{1+(k\delta/2)^2}\,; \tag{9.4}$$

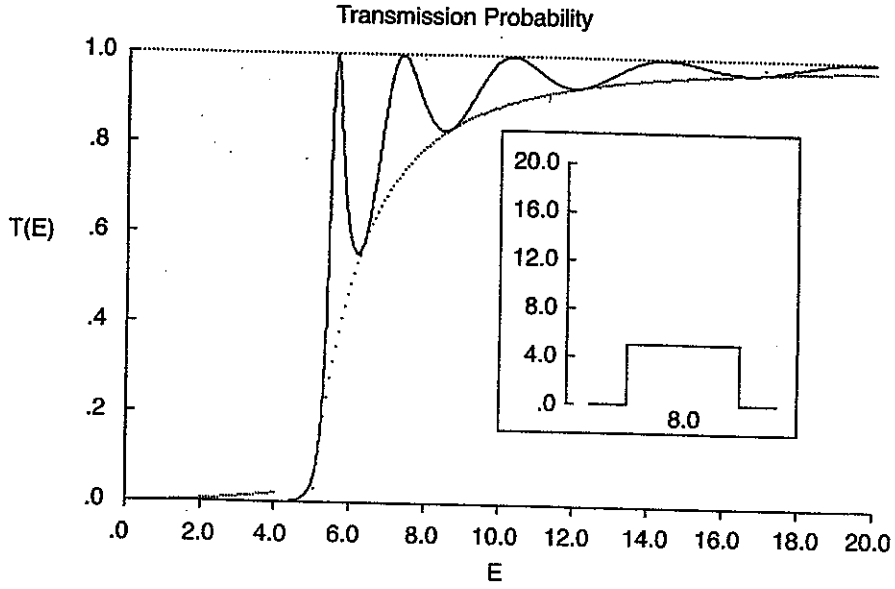

Fig. 9.1 Transmission probability, $T(E)$, as a function of energy for an incident electron of energy E on the barrier shown in the inset. The barrier has height 5 eV, width 8 Å. The transmission probability is computed using the analytic expressions (9.1)–(9.6). Shown also are the asymptotic estimate for the tunneling probability given in (9.9) (dotted, to 4 eV) and the lower bound on the transmission probability given by the expression (9.12), (dotted, $E > V$).

$$E > V\text{: } k' = \sqrt{2m(E-V)/\hbar^2},$$

$$t_{11}(E) = \cos k'\delta - \frac{i}{2}\left(\frac{k'}{k} + \frac{k}{k'}\right)\sin k'\delta\,, \tag{9.5}$$

$$T(E) = \frac{1}{\cos^2 k'\delta + \frac{1}{4}\left(\frac{k'}{k} + \frac{k}{k'}\right)^2 \sin^2 k'\delta} = \frac{1}{1 + \frac{1}{4}\left(\frac{k'}{k} - \frac{k}{k'}\right)^2 \sin^2 k'\delta}\,. \tag{9.6}$$

The identities $\cosh^2 x - \sinh^2 x = 1$, $\cos^2 x + \sin^2 x = 1$ have been used to construct $T(E)$ from $t_{11}(E)$ in the cases $E < V, E > V$.

The transmission probability $T(E)$ is plotted as a function of E in Fig. 9.1 for the repelling barrier shown in the inset. The behavior of the transmission probability is not exactly intuitive for anyone whose intuition is developed on classical (= nonquantum) mechanics. Classically, a particle with energy $E < V$ will be reflected at the barrier

with 100% probability. When $E > V$ it will be transmitted with 100% probability.[1] We observe that for $E > V$ the transmission probability is exactly 1 only at isolated points, which are the zeros of $\sin k'\delta$.

There is always a nonzero probability for transmission through the barrier even in the classically forbidden regime $E < V$, where the classical particle is reflected. Transmission through a classically forbidden region is called quantum mechanical tunneling, or simply tunneling.

The transmission probability is not reduced to zero by making the barrier thicker or higher, although it may be dramatically reduced. The asymptotic behavior of the transmission probability through this barrier is simple to discuss. In the classically forbidden regime $E < V$, $\kappa\delta = \sqrt{2m(V-E)/\hbar^2}\delta$ and

$$\sinh \kappa\delta \quad \rightarrow \quad \frac{1}{2}e^{\kappa\delta}\,, \tag{9.7}$$

$$\left(\frac{\kappa}{k}+\frac{k}{\kappa}\right)^2 \quad = \quad \frac{V-E}{E}+2+\frac{E}{V-E}=\frac{V^2}{E(V-E)}\,. \tag{9.8}$$

Using these approximations in the expression for $T(E)$ given in (9.2), and neglecting "1" compared with the larger term, the asymptotic dependence of the transmission probability is

$$T(E) \overset{\kappa\delta\gg 1}{\longrightarrow} 16\frac{E(V-E)}{V^2}\,e^{-2\kappa\delta}\,. \tag{9.9}$$

This argument shows that in the classically forbidden regime the transmission probability drops off exponentially, so that

$$\log\, T(E) \sim -2\kappa\delta = -2\sqrt{2m(V-E)/\hbar^2}\,\delta\,. \tag{9.10}$$

In the classically allowed regime $E > V$ the transmission probability (9.6) is +1 only at isolated energies at which $\sin k'\delta = 0$, or $k'\delta = n\pi$. Since $k' = \sqrt{2m(E-V)/\hbar^2}$, these occur at energies

$$E_n = V + \frac{\hbar^2}{2m}\left(\frac{n\pi}{\delta}\right)^2 \qquad n = 1, 2, \ldots\,. \tag{9.11}$$

However, as the energy increases, the transmission probability gets closer and closer to +1. In fact, it oscillates between the upper and lower bounds

$$\begin{aligned} T_{\text{upper bound}} \quad &= \quad 1\,, \\ T_{\text{lower bound}} \quad &= \quad \frac{1}{1+\frac{1}{4}\left(\frac{k'}{k}-\frac{k}{k'}\right)^2} = 1-\left(\frac{V}{2E-V}\right)^2\,. \end{aligned} \tag{9.12}$$

[1]This is strictly true only if the barrier height is a sufficiently slowly varying function of position. A classical bowling ball with $E > V$ could not pass the barrier in the inset of Fig. 9.1 unless the corners were rounded considerably.

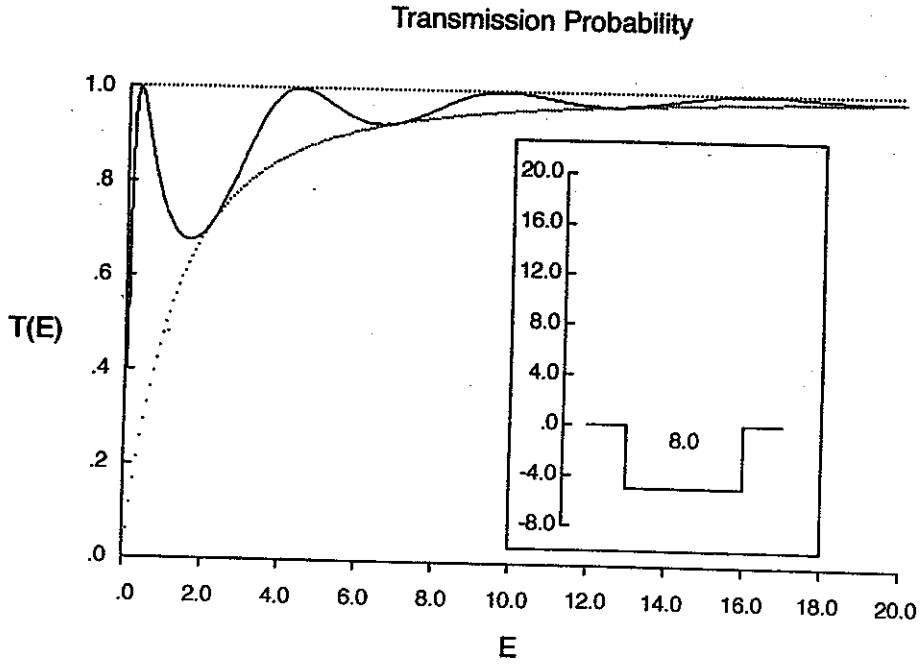

Fig. 9.2 Transmission probability as a function of incident energy for the "attracting barrier" ($V = -5$ eV) shown in the inset. Upper and lower bounds on $T(E)$ are shown by dotted lines.

For $E \gg V$ the lower bound approaches the upper bound algebraically (i.e., power law behavior) and the system behaves classically.

It is a simple matter to verify that as E approaches V from below, $T(E)$ given by (9.2) approaches the grazing limit $T(E) = [1+(k\delta/2)^2]^{-1}$ given by (9.4). Similarly, as E approaches V from above, the limit of $T(E)$ given by (9.6) also approaches this grazing limit.

The transmission probability for an "attracting barrier" has also been computed, and is shown in Fig. 9.2. For this barrier, $V_L = V_R = 0, V < 0$, so the transmission probability is given by

$$\begin{aligned} k &= \sqrt{2mE/\hbar^2}\,, \\ k' &= \sqrt{2m(E-V)/\hbar^2} = \sqrt{2m(E+|V|)/\hbar^2}\,, \\ T(E) &= \frac{1}{1+\frac{1}{4}\left(\frac{k'}{k}-\frac{k}{k'}\right)^2 \sin^2 k'\delta}\,. \end{aligned} \tag{9.13}$$

The bounds on the transmission probability are as given in (9.12).

Equation (8.3)
tion probabilit
for the simples
ements analyti
The algorithm

- Read in
  as the as
- Choose
- Comput
- Multipl
  $M(E)$ =
- Comput

For many pur
energy. This r
that scans ove

In Fig. 10.
for a particle c
simple barrier
Fig. 9.1. The
offset above t
$T(E)$. A simi
previously in

10

Coding and Validation

Equation (8.3) provides a simple algorithm for computing the transmission and reflection probabilities from the matrix elements of the transfer matrix. However, except for the simplest cases (previous chapter) it is not practical to compute these matrix elements analytically. It is therefore useful to carry out such computations numerically. The algorithm for this numerical computation is straightforward:

- Read in the height V_j and width δ_j of the piecewise constant potential, as well as the asymptotic potential values V_L, V_R on the left and right.
- Choose a value, E, for the incident particle energy ($E > V_L, E > V_R$).
- Compute the real 2×2 matrix $M(V_j; \delta_j)$ for each piece of the potential.
- Multiply these matrices in the order in which they occur, from left to right: $M(E) = \prod_{j=1}^{j=N} M(V_j; \delta_j)$.
- Compute $t_{11}(E)$ in terms of $m_{ij}(E), k_L, k_R$ using (8.8) or (8.9).

For many purposes it is useful to compute $T(E)$ as a function of the incident particle energy. This means that the computation outlined above must be embedded in a loop that scans over the desired range of values of the incident particle energy.

In Fig. 10.1 we present the numerically computed transmission probability, $T(E)$, for a particle of energy E incident on the barrier shown in the inset. Since this is a very simple barrier, the results are available analytically and have already been plotted in Fig. 9.1. These analytic results are also presented in Fig. 10.1 (dotted curve, slightly offset above the solid curve), for comparison with the numerically computed value of $T(E)$. A similar comparison is made in Fig. 10.2 for the attracting potential treated previously in Fig. 9.2.

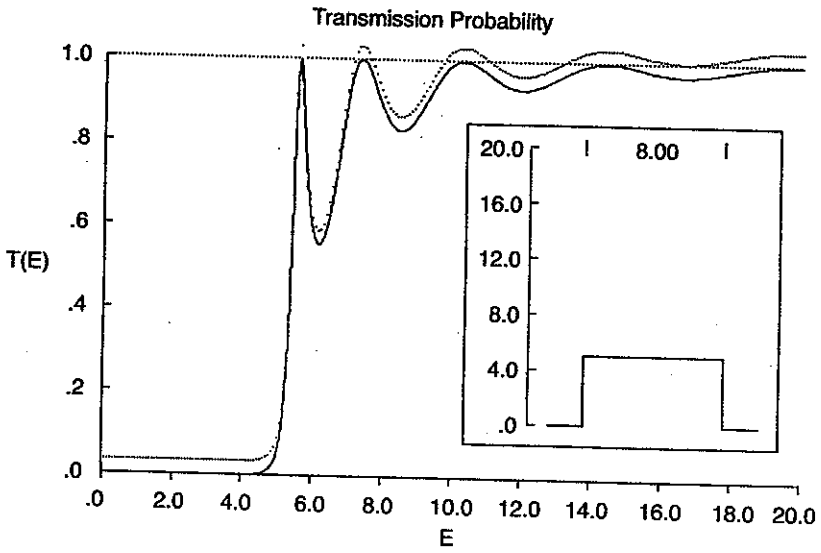

Fig. 10.1 Transmission probability, $T(E)$, computed numerically for an incident electron of energy E, for the potential barrier shown in the inset. This is to be compared with the analytic computation presented in Fig. 9.1. That curve is shown in this figure, dotted and slightly displaced above the numerically computed curve. The two curves are identical.

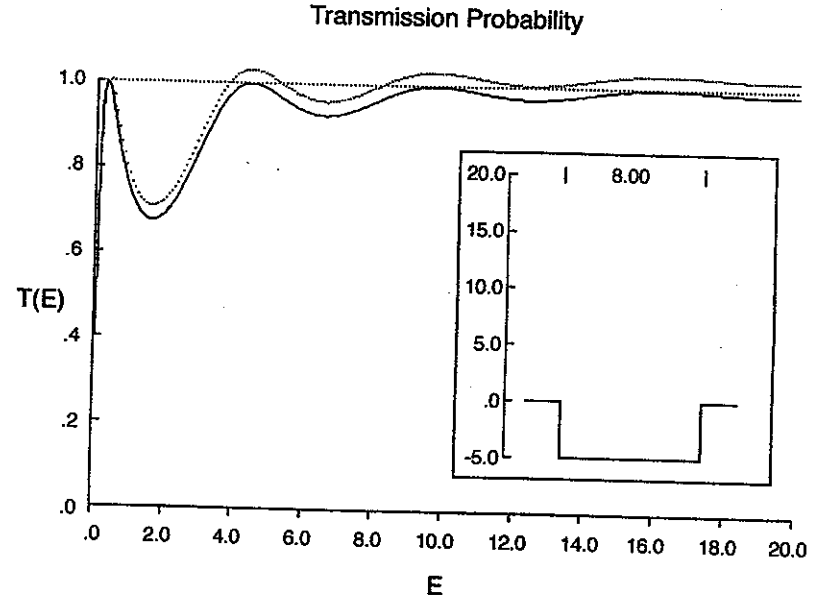

Fig. 10.2 Numerically computed transmission probability for the "attracting barrier" shown in the inset. The curve from the analytic computation (Fig. 9.2) is shown dotted and slightly offset. The two curves are identical.

The plots of
single rectang
the classical r
+1. These pe
We should
intrinsic to qu
potential shap
regions. To ac
for two smoo
The smoot

We study this
$x = -2$ to x
piecewise cor
of $V(x) = V$
In Fig. 11.
eV in the inte
potential appr
structure abo
remains.
In Fig. 11.
approximatio
has been rem

11

Shape of Barrier

The plots of transmission probability versus energy given in Figs. 9.1–10.2 for a single rectangular barrier show a lot of structure. In particular, they exhibit peaks in the classical region ($E > V$) at which the transmission probability assumes the value +1. These peaks are suggestive of a "resonance structure" (see chapter 16).

We should wonder what part of the structure shown in the $T(E)$ versus E plots is intrinsic to quantum mechanical systems, and what part is an artifact of the particular potential shape chosen, with "square corners" and discontinuities between separate regions. To addess this question we study the transmission probability spectrum $T(E)$ for two smoother potentials.

The smooth scattering potential that we study has a Gaussian shape:

$$V(x) = Ve^{-x^2}\,, \qquad -4 \leq x \leq +4\,. \tag{11.1}$$

We study this potential by making a piecewise approximation to it. The interval from $x = -2$ to $x = +2$ is divided into N (odd) equal length intervals. The value of the piecewise constant potential in the jth interval ($1 \leq j \leq N$) is chosen to be the value of $V(x) = V\ e^{-x^2}$ at the midpoint of that interval.

In Fig. 11.1 we plot $T(E)$ for a five-piece approximation to this potential for $V = 5$ eV in the interval $0 < E \leq 20$ eV. The inset shows how well the piecewise constant potential approximates the smooth potential. We see from this plot that most of the structure above $V = 5$ eV has been washed out, but that some residual structure still remains.

In Fig. 11.2 we repeat the calculation shown in Fig. 11.1, but for an eleven-piece approximation to this smooth potential. Essentially all the structure above $E = V$ has been removed by this eleven-piece approximation to the smooth potential. The

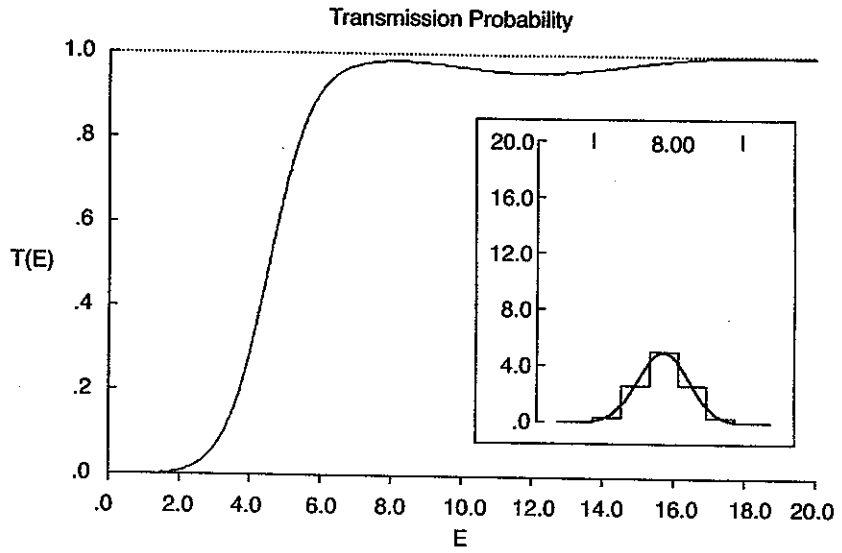

Fig. 11.1 Transmission probability for the five-piece approximation to the smooth repelling Gaussian potential shown in the inset.

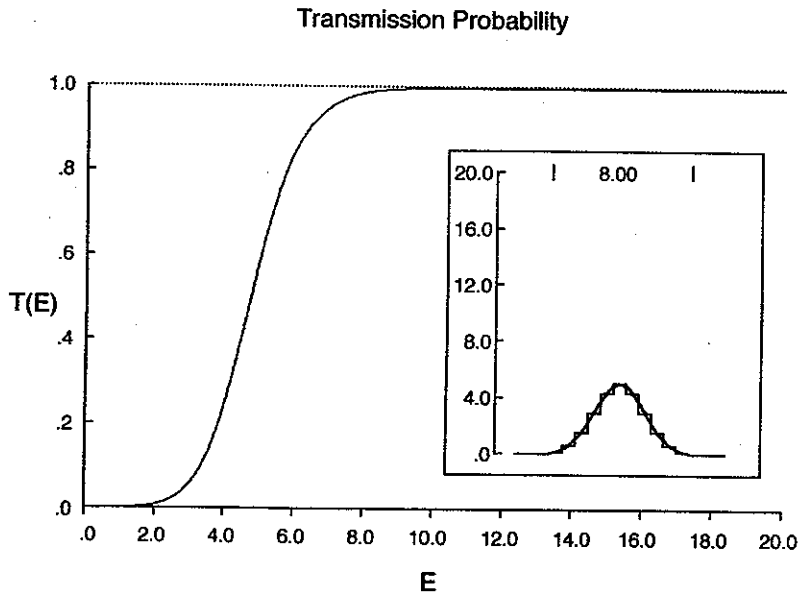

Fig. 11.2 Transmission probability for the eleven-piece approximation to the smooth repelling Gaussian potential shown in the inset. The resonance structure that appears in Figs. 9.1 and 10.1 for the one-piece approximation to the smooth potential is washed out in this smoother approximation.

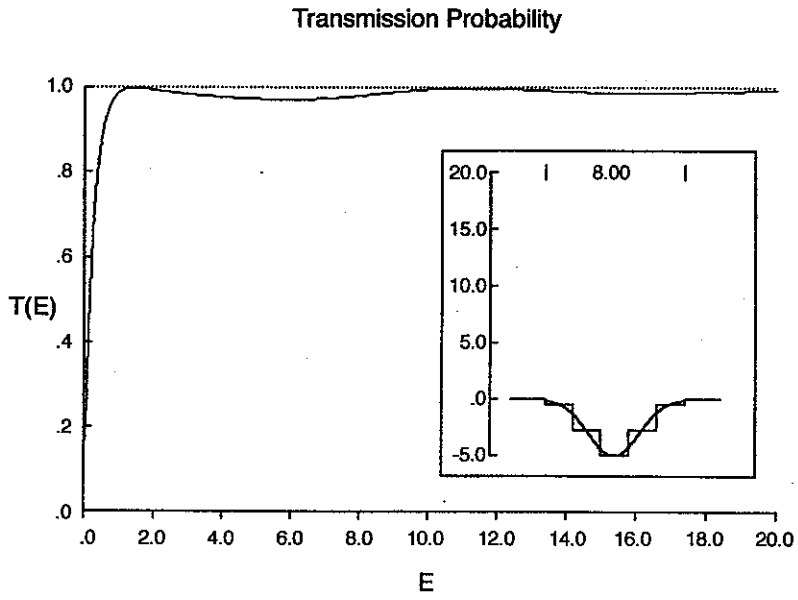

Fig. 11.3 Transmission probability for the five-piece approximation to the smooth attracting Gaussian potential shown in the inset.

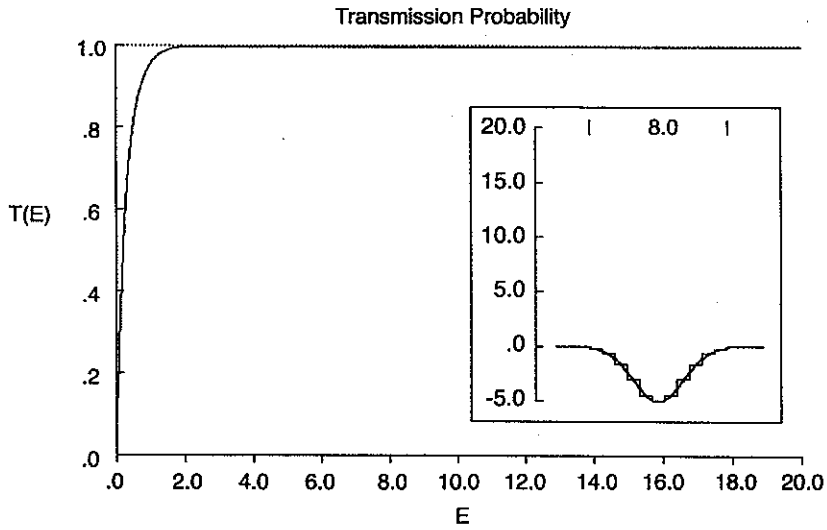

Fig. 11.4 Transmission probability for the eleven-piece approximation to the smooth attracting Gaussian potential shown in the inset. The resonance structure which appears in Figs. 9.2 and 10.2 for the one-piece approximation to the smooth potential is washed out in this smoother approximation.

$T(E)$ versus E curve does not show any additional changes as the approximation improves (to $N = 101$).

A similar set of computations was done for the attracting potential "barrier," $V(x) = Ve^{-x^2}, V < 0$. The results are shown for $V = -5$ eV, for five- and eleven-piece approximations to this inverted Gaussian potential, in Figs. 11.3 and 11.4. We again see that the resonance structure, apparent in Figs. 9.2 and 10.2 for the attracting square well, becomes washed out as we make better and better piecewise constant approximations to the smooth potential.

The calculations done here suggest that some of the features apparent in the transmission probability computed for a square well scattering or binding potential (Figs. 9.1 through 10.2) are artifacts due to the discontinuities between potentials in adjacent regions. As the discontinuities become smaller, the structures they produce also diminish.

However, there is one feature that is not an artifact of the shape of the potential. This is the depression of $T(E)$ below one for an attracting barrier that occurs at small energy. That is, the dip near $E = 0$ that occurs in Figs. 9.2 and 10.2 is still present (Figs. 11.3 and 11.4) in the five- and eleven-piece approximations to the inverted Gaussian potential. This is not an artifact of our computational procedure: this phenomenon is exhibited by real quantum mechanical systems.

In this chapte
bility under tv
scattering pot
The argum
through a clas
where L is the
square well b
sufficiently la
In Fig. 12.
$L = 1$ Å, $E =$
shows linear b
These resu
has the form

The integral is
$x \leq b$.
In Fig. 12.
potential shov
of width $L = 1$
13-piece appr

12

Asymptotic Behavior

In this chapter we investigate the asymptotic behavior of the transmission probability under two different conditions. These conditions involve tunneling through a scattering potential and transmission through an attracting potential.

The arguments leading to equation (9.9) suggest that the transmission probability through a classically forbidden region behaves exponentially like $T(E) \sim e^{-2\kappa L}$, where L is the width of the potential. In Fig. 12.1 we plot $\ln [T(E)]$ versus L for the square well barrier shown in the inset. This clearly shows linear behavior in L for sufficiently large L ($L > 1$ Å). For this calculation, $V = 5.0$ eV, $E = 4.0$ eV.

In Fig. 12.2 we plot $\ln [T(E)/T(V)]$ as a function of $\kappa = \sqrt{2m(V-E)/\hbar^2}$ for $L = 1$ Å, $E = 4.0$ eV, where V is varied from $E + 0.0001$ eV to 105.0 eV. This also shows linear behavior in κ for κ sufficiently large ($\kappa > 2$ Å^{-1}).

These results suggest an asymptotic behavior for the tunneling probability, which has the form

$$\begin{aligned} T(E) &\sim \left| \exp - \int_a^b \kappa(x) dx \right|^2 \\ &= \exp -2 \int_a^b \sqrt{2m(V(x)-E)/\hbar^2}\, dx \,. \end{aligned} \tag{12.1}$$

The integral is carried out through the classically forbidden region $V(x) - E \geq 0, a \leq x \leq b$.

In Fig. 12.3 we plot $-\ln\ T(E)$ versus $2\int_a^b \kappa(x)dx$ for the Gaussian scattering potential shown in the inset. The calculations have been carried out for potentials of width L= 1, 3, 5, 7, 9 Å, of height V = 5, 15, $\cdots$, 105 eV, using N = 1-, 5-, 9-, 13-piece approximations to this potential. The incident particle energy was scanned in

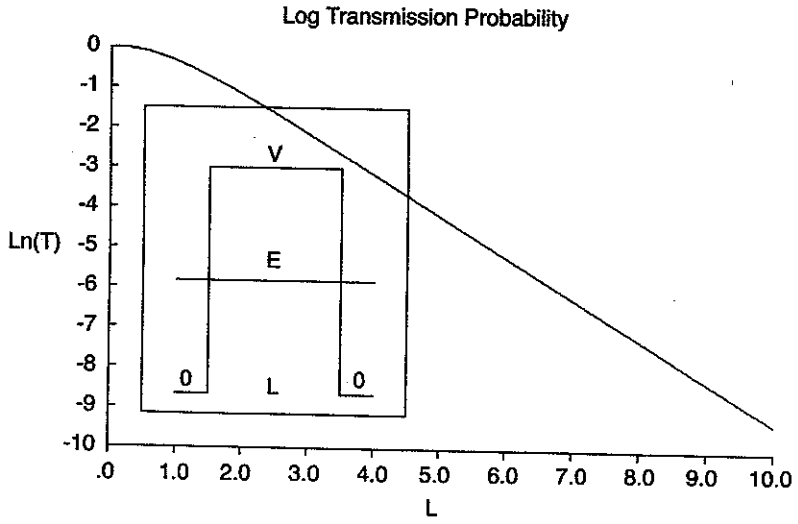

Fig. 12.1 Natural logarithm of the transmission probability decreases linearly with the width of the barrier, for sufficiently wide barriers. Parameter values for this plot: $V = 5.0$ eV, $E = 4.0$ eV.

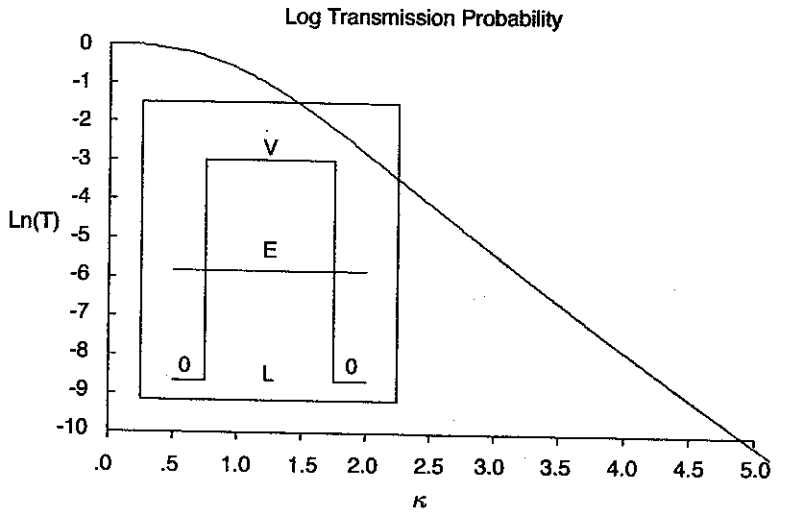

Fig. 12.2 Natural logarithm of the transmission probability decreases linearly with κ for sufficiently large values of κ. For this plot $E = 4.0$ eV, $L = 1.0$ Å, and the barrier potential is scanned from slightly above E ($V = E + 0.0001$ eV) to $V = 105.0$ eV. The transmission probability has been normalized by dividing by the transmission probability at the grazing energy, $T(E = V)$.

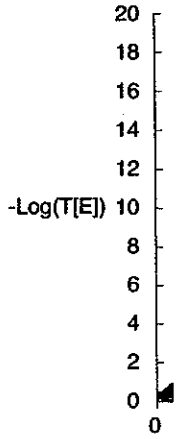

Fig. 12.3 Natural l
for a large number of

the range of energi
left and right are V
the scanning variabl
constant approxima
washed out.

The asymptotic
barrier are simple to
($E \sim 0$) the transm
computational proc

To get some indi
Gaussian potential
computation was d
$N = 101$ pieces. T
for two energies, E
behavior are appare
these two figures w
peaks become narr
each peak becomes
successive spikes q

We will see later
formation of new b

Problem. Comp
E.

Problem. Comp
two lowest peaks (e

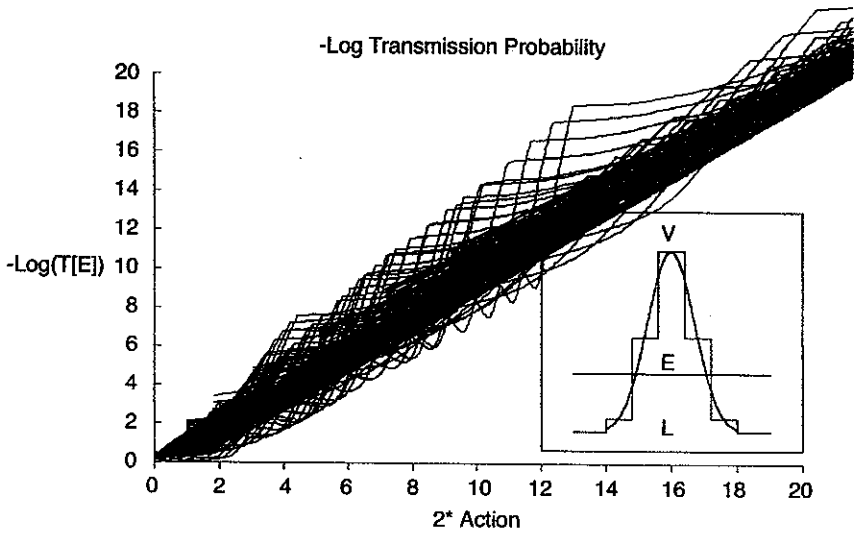

Fig. 12.3 Natural logarithm of the transmission probability is plotted against $\int_a^b \kappa(x)\,dx$ for a large number of approximations to the smooth potential shown.

the range of energies +1 eV $\leq E \leq (V - 1)$ eV. The asymptotic energies on the left and right are $V_L = V_R = 0$. The sharp kinks are related to the passage of the scanning variable E through the discontinuities that are apparent in the piecewise constant approximation to the smooth potential. As N increases, the kinks become washed out.

The asymptotic properties of the transmission probability through an attracting barrier are simple to discuss. For most energies, $T(E) \sim 1$. However, for low energy ($E \sim 0$) the transmission probability exhibits structure that is not an artifact of our computational procedure.

To get some indication of this structure, we have computed $T(E)$ for the attracting Gaussian potential $V(x) = Ve^{-x^2}$ (-20 eV $< V < 0$ eV, -4 Å $\leq x \leq +4$ Å). The computation was done using a piecewise constant approximation to $V(x)$ involving $N = 101$ pieces. The calculations were done at many energies. We show the results for two energies, $E = 0.1$ eV (Fig. 12.4) and $E = 0.01$ eV (Fig. 12.5). The trends in behavior are apparent from these figures. As E increases, the structure exhibited in these two figures washes out (cf. also Figs. 11.3, 11.4). As the energy decreases, the peaks become narrower and the minima between them become deeper. As $E \to 0^+$ each peak becomes an infinitely thin spike and the transmission probability between successive spikes quickly approaches zero.

We will see later (Part III, chapter 25) that these peaks are intimately related to the formation of new bound states in potentials of finite depth.

Problem. Compute the width of the lowest peak ($V = -2.2$ eV) as a function of E.

Problem. Compute the asymptotic form of $T(E)$ as a function of E between the two lowest peaks (excluding the peak at $|V| = 0$) at about $V = -5.5$ eV.

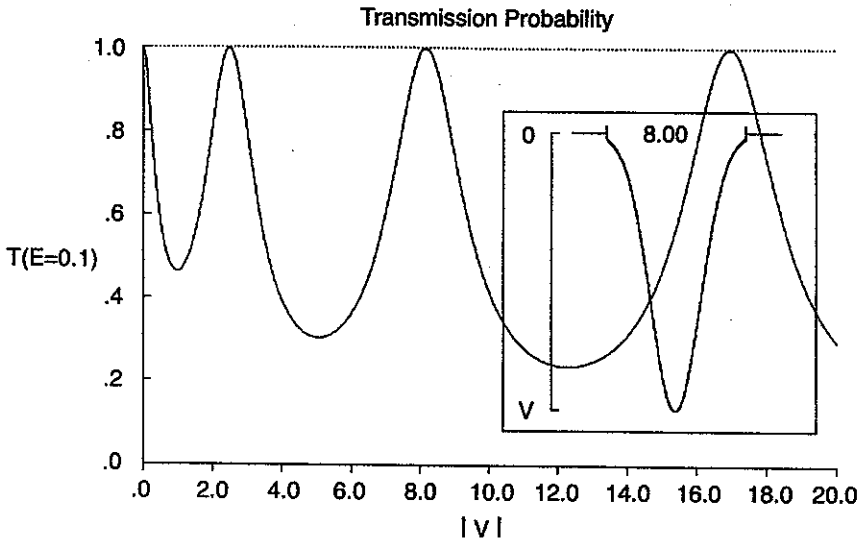

Fig. 12.4 Transmission probability for incident electron energy $E = 0.1$ eV for attracting potentials (inset) of various depth.

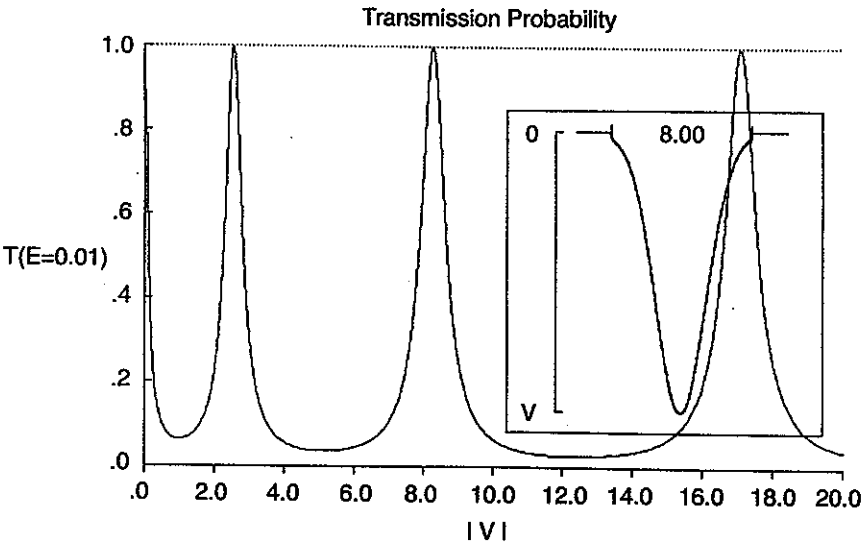

Fig. 12.5 Transmission probability for incident electron energy $E = 0.01$ eV for attracting potentials of various depth. The sharp peaks at low scattering energy are closely related to the bound states that this potential possesses.

Scattering phenome
than tunneling, and
the phenomenon of

For a target for v
a complex function

For the single barri
$t_{11}(E)$ (see (9.5))

where $k = \sqrt{2mE}$
by taking the ratio

It is not entirely strai
$\tan(\phi + n\pi) = \tan$
equation. However,

$E = 0.1$ eV for attracting

$E = 0.01$ eV for attracting
gy are closely related to the

13

Phase Shifts

Scattering phenomena exhibit another type of asymptotic behavior that is more subtle than tunneling, and which deserves to be discussed in a chapter of its own. This is the phenomenon of scattering phase shifts.

For a target for which $V_L = V_R = 0$, $T(E) = |1/t_{11}(E)|^2$. In general, $t_{11}(E)$ is a complex function that we can write as

$$t_{11}(E) = \frac{1}{\sqrt{T}}\, e^{-i\phi}\,. \tag{13.1}$$

For the single barrier of potential $V(< E)$ and width L, we have already computed $t_{11}(E)$ (see (9.5))

$$t_{11}(E) = \cos k'L - \frac{i}{2}\left(\frac{k'}{k} + \frac{k}{k'}\right)\sin k'L\,, \tag{13.2}$$

where $k = \sqrt{2mE/\hbar^2}, k' = \sqrt{2m(E-V)/\hbar^2}$. The angle $\phi(E)$ can be determined by taking the ratio of the imaginary to real values in (13.1) and (13.2):

$$\tan\phi = \frac{1}{2}\left(\frac{k'}{k} + \frac{k}{k'}\right)\tan k'L\,. \tag{13.3}$$

It is not entirely straightforward to solve this equation for ϕ. This comes about because $\tan(\phi + n\pi) = \tan\phi$ (n integer), so that many different values of ϕ can satisfy this equation. However, we recognize that as long as $k, k' \neq 0, \infty$

$$\begin{aligned} \tan\phi = 0 \quad &\Longleftrightarrow \quad \tan k'L = 0\,, \\ \cot\phi = 0 \quad &\Longleftrightarrow \quad \cot k'L = 0\,. \end{aligned} \tag{13.4}$$

Therefore, as we change parameter values (E, V, L) we can determine that ϕ is within $\pm\pi/2$ radians of $k'L$. In particular, we determine

$$\phi = \tan^{-1}\left(\frac{1}{2}\left(\frac{k'}{k} + \frac{k}{k'}\right)\tan k'L\right) + \pi\left[\frac{k'L}{\pi} + \frac{1}{2}\right] \tag{13.5}$$

The complicated form of this expression comes about for two reasons:

1. The principal value of the $\tan^{-1}$ function is in the range $-\pi/2 < \phi < +\pi/2$.
2. The "greatest integer" function ($[x]$) truncates the decimal part of a real number x, rather than rounding to the nearest integer.

We show in Fig. 13.1 a plot of $\phi/2\pi$ against $k'L/2\pi$ for the potential shown in the inset. We expect $\phi(E)$ to intersect the diagonal ($\phi = k'L$) at integer values by (13.4). This in fact occurs. However, this plot holds two surprises:

1. $\phi(E)$ behaves asymptotically like $k'L$ even for relatively small values of $k'L$ $(k'L/2\pi > 2)$.
2. $\phi(E)$ shows significant structure for $k'L$ small $(0 < k'L/2\pi < 1)$.

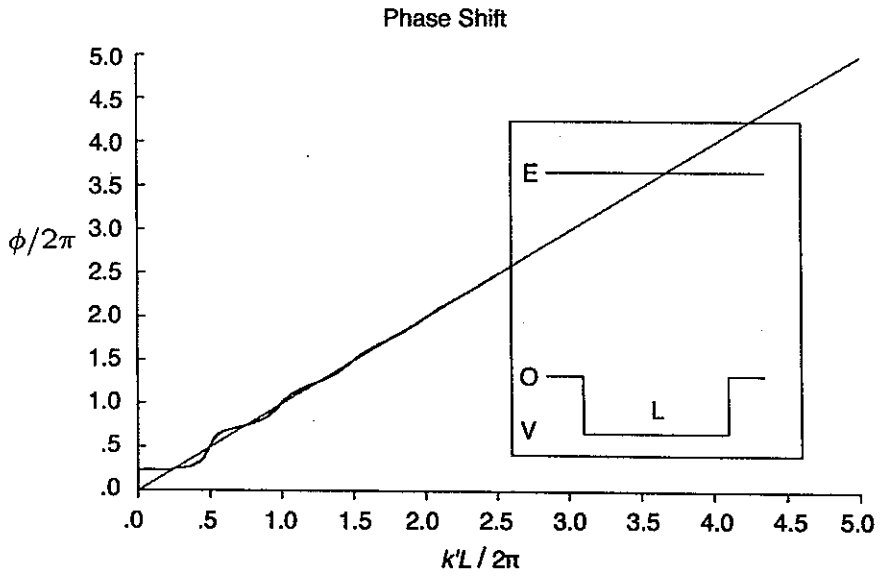

Fig. 13.1 Phase shift $\phi/2\pi$ of a particle with incident energy E as a function of $k'L/2\pi$, the action on traversing the barrier shown. For this calculation, $E = 100.0$ eV, $L = 4.0$ Å, and V is scanned from just below 100 eV to large negative values.

What does this phase mean physically? To answer this question, we compute ϕ when there is no scattering potential at all ($V = V_L = V_R = 0$). Then $k = k'$ and

$$\begin{aligned} t_{11}(E) &= \cos k'L - \frac{i}{2}\left(\frac{k'}{k} + \frac{k}{k'}\right)\sin k'L \\ &= \cos kL - i\sin kL = e^{-ikL} . \end{aligned} \tag{13.6}$$

Thus, $\phi = kL$. This is exactly the change in phase that occurs as the particle moves from one side of the "potential" at $x = a_L$ to the other side at $x = a_R$ through a distance L, for

$$\begin{aligned} \Phi(x)|_{x=a_R} &= A\, e^{ika_R} = A\, e^{ik(a_R - a_L + a_L)} \\ &= e^{ikL}\, \Phi(x)|_{x=a_L} . \end{aligned} \tag{13.7}$$

For more complicated potentials

$$t_{11}(E) = \frac{1}{\sqrt{T}}\, e^{-i\phi} = \frac{1}{2}\left(m_{11} + \frac{k_R}{k_L} m_{22}\right) + \frac{i}{2}\left(k_R m_{12} - \frac{m_{21}}{k_L}\right) . \tag{13.8}$$

In a typical scattering experiment $V_L = V_R = 0$, $k_L = k_R = k_0$, and the phase shift is given, up to an integer multiple of π, by

$$\phi = \tan^{-1}\left(\frac{-k_0 m_{12} + m_{21}/k_0}{m_{11} + m_{22}}\right) . \tag{13.9}$$

In the classically allowed regime where reflection can be neglected, the expression for the phase shift is well approximated by

$$\phi = \int_a^b k(x)dx . \tag{13.10}$$

This can be approximated, for $E = \hbar^2 k_0^2/2m$, by

$$\phi = \int_a^b \sqrt{2m(E - V(x))/\hbar^2}\; dx \simeq k_0 L\left(1 - \frac{\overline{V}}{2E}\right) . \tag{13.11}$$

Here the average energy is defined by $\overline{V} = \int_a^b V(x)dx/L$, with $L = b - a$. This shows that the phase shift over a length L is monotonically increasing and asymptotically approaches $k_0 L$ for sufficiently large energies.

In Figs. 13.2 and 13.3 we show the phase shift for an electron incident on an attracting and a repelling Gaussian potential $V(x) = V_0 e^{-(x/2)^2}$, $V_0 = \mp 5$ eV. An eleven-piece approximation to the potential is shown in the inset. The phase shift $\phi(E)$ is plotted both as a function of the parameter $k_0 L$ (curve a) and $\int_{-4}^{+4} k(x)dx$ for the attracting potential ($V_0 = -5$ eV), and the real part of this this integral for the potential barrier ($V_0 = +5$ eV) (curve b). Curves a and b approach each other asymptotically as E becomes sufficiently large.

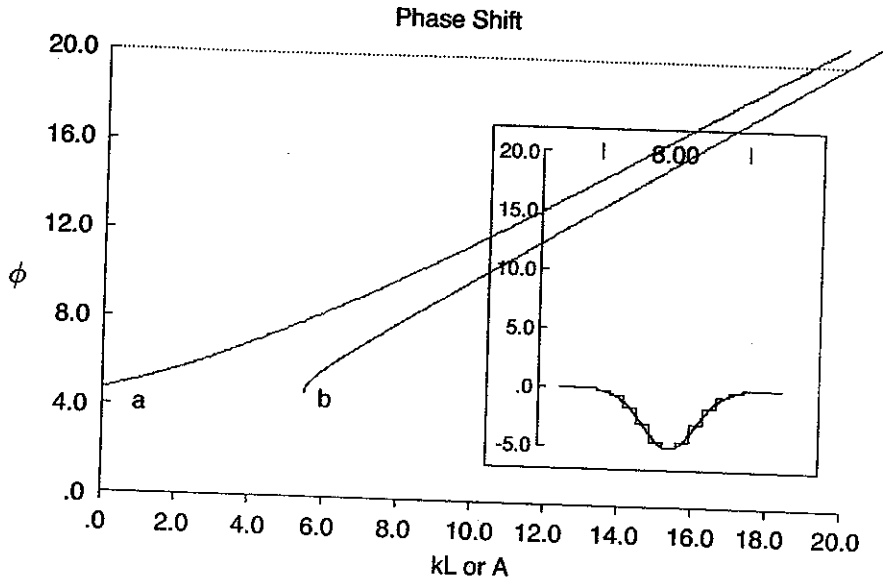

Fig. 13.2 Phase shift ϕ for the attracting barrier (inset) plotted as a function of (a) $k_0 L$ and (b) action integral $A = \int k(x)dx$. The phase shift at $E = 0$ is positive since the particle speeds up on passing through the potential.

We point out that the phase shift at zero energy is positive for the attracting potential and negative for the repelling potential.

Problem. Show that the tunneling results ($E < V$) and the phase shift results ($E > V$) can be put into the following similar form

$$t_{11}(E) \sim \exp -i \int_a^b \sqrt{2m(E - V(x))/\hbar^2}\, dx$$
$$= \exp -\frac{i}{\hbar} \int_a^b p(x)\, dx\,, \qquad (13.12)$$

where $V(a) = V(b) = E, p(x) = \sqrt{2m(E - V(x))}$ and the appropriate square root is taken when $E - V(x) < 0$. The integral $A = \int_a^b p(x)\, dx$ is called the *classical action* of the particle.

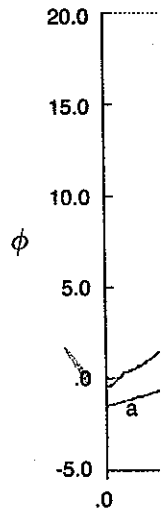

Fig. 13.3 Phase
(b) action integral
down on passing t

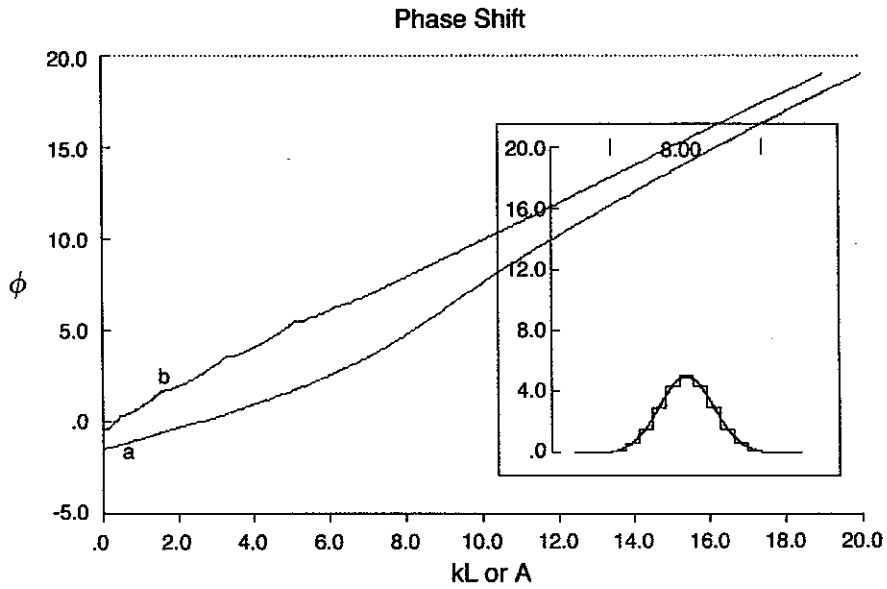

Fig. 13.3 Phase shift ϕ for the repelling barrier (inset) plotted as a function of (a) k_0L and (b) action integral $A = \int k(x)dx$. The phase shift at $E = 0$ is negative since the particle slows down on passing through the potential.

14

Double Barrier

Up to now we have considered tunneling problems for which the classically forbidden region is one contiguous region. In such cases we have seen that the transmission probability has an asymptotic form

$$T(E) \sim \exp\left[-2\int_a^b \sqrt{\frac{2m(V(x)-E)}{\hbar^2}}\,dx\right] . \tag{14.1}$$

This asymptotic form is no longer accurate when the classically forbidden region consists of two or more disjoint pieces. Then resonances can occur between adjacent classically forbidden regions that alter $T(E)$ in a very significant way.

We illustrate what can occur by computing the transmission probability for the double well potential shown in Fig. 14.1 (inset). The remarkable feature to be observed is that the transmission probability is very large, in fact +1, for certain values of the energy for which transmission is classically forbidden. The potential shown has two barriers of height $V = 5$ eV and width $D = 2$ Å separated by a region at 0 eV and width $L = 6$ Å; $V_L = V_R = 0$. It appears that the lowest peak does not reach $T(E) = 1.0$. However, this is a resolution problem. The peak is so narrow that the energies for which $T(E)$ was computed (every 0.002 eV) only sampled the shoulder of this peak.

A number of questions should naturally be asked. These include:

- Why does this phenomenon occur?
- How are the location and width of the peaks related to the parameters of the potential?

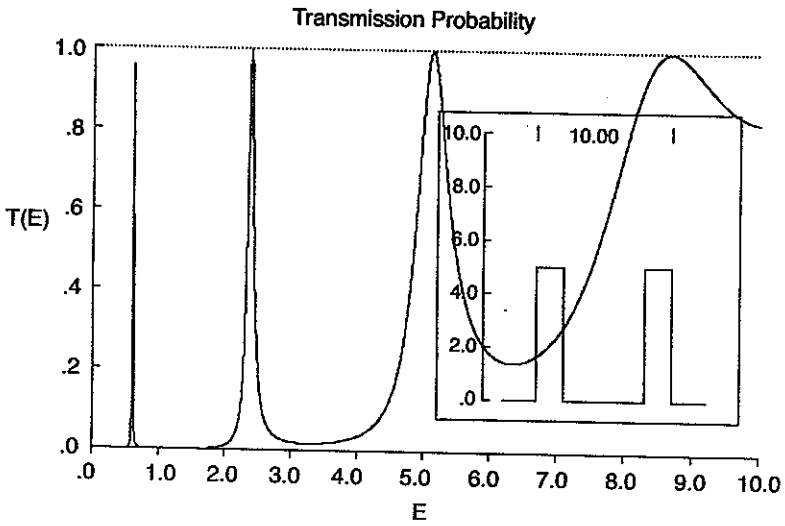

Fig. 14.1 Transmission probability spectrum for double barrier scattering potential shown in inset. The two identical barriers have width 2 Å and height 5 eV. They are separated by 6 Å. The peak at 0.6 eV is not completely resolved at the energy resolution (0.002 eV) used for this computation.

- What is the shape of the peaks?

We will answer these questions in reverse order. Briefly, we show in the remainder of this chapter that the peaks have a Lorentzian line shape. We leave it to the first problem at the end of this chapter to show that the peaks occur at energies $E_n \sim \frac{\hbar^2}{2m}\left(\frac{n\pi}{L}\right)^2$, where L is the width of the intermediate classically allowed region. In the second problem we show that the width of the peaks decreases exponentially with the thickness, D, of the classically forbidden region. In chapter 16 we show that this phenomenon is due to the occurrence of resonances within the classically allowed regions.

In order to show that the peak at $E \sim 0.6$ eV in Fig. 14.1 really rises to $T(E) = 1$ for some value of E, we have resolved the peak by scanning the energy from $E = 0.59$ eV to $E = 0.64$ eV in 500 steps. The shape of this lowest resonance is shown in Fig. 14.2. This clearly has a maximum at $T(E) = 1$ for $E \simeq 0.615$ eV.

Two reasonable candidates for describing the bell-shaped curve are the Gaussian function and the Lorentzian function. We could try to fit the data in Fig. 14.2 to each type of curve and then determine how good or bad the fit is. This is a standard problem of statistics. We will not pursue this approach here. Rather, we will determine the consequences of each functional form and compare these consequences to the data.

Gaussian. If the curve shown in Fig. 14.2 is a Gaussian, it has the form

$$T(E) = Ae^{-[(E-E_0)/\Delta E]^2}, \tag{14.2}$$

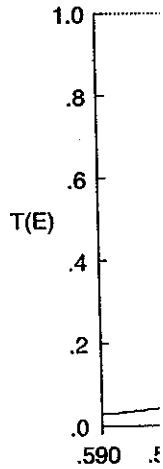

Fig. 14.2 Lowest p
higher resolution (ΔE

where E_0 is the loc
the negative logarit

The first derivative

Fig. 14.3 repeats t
versus E (looks lik
The first derivative
that the resonance
Lorentzian. If

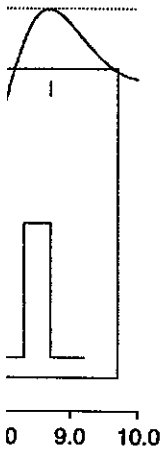

attering potential shown
They are separated by 6
tion (0.002 eV) used for

how in the remainder
Ve leave it to the first
ur at energies $E_n \sim$
y allowed region. In
es exponentially with
16 we show that this
e classically allowed

lly rises to $T(E) = 1$
nergy from $E = 0.59$
sonance is shown in
.615 eV.
rve are the Gaussian
a in Fig. 14.2 to each
is a standard problem
e will determine the
quences to the data.
as the form

(14.2)

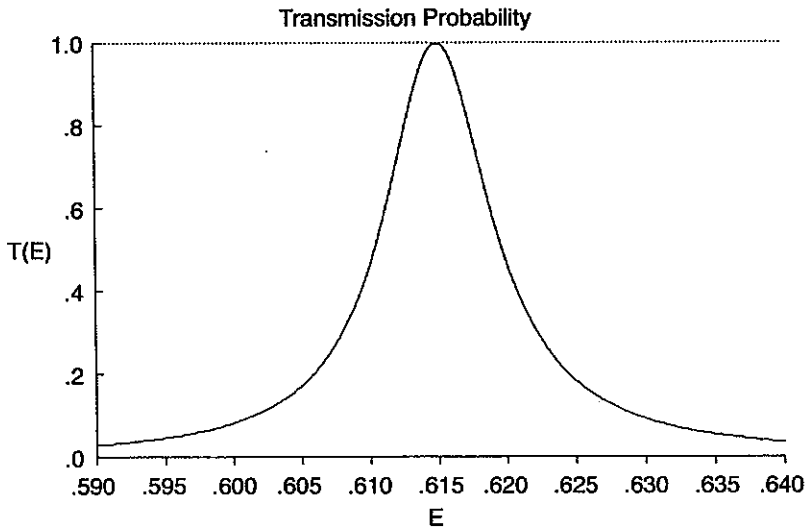

Fig. 14.2 Lowest peak in the transmission spectrum shown in Fig. 14.1 is resolved by a higher resolution ($\Delta E = 0.0001$ eV) energy scan.

where E_0 is the location of the peak and ΔE is related to its half width. By taking the negative logarithm we should have a rising parabola

$$-\ln T(E) = \left(\frac{E - E_0}{\Delta E}\right)^2 - \ln A\,. \tag{14.3}$$

The first derivative is a linear function, and the second is a constant:

$$\begin{aligned} \frac{d}{dE}(-\ln T) &= 2\left(\frac{E - E_0}{\Delta E}\right)\frac{1}{\Delta E}\,, \\ \frac{d^2}{dE^2}(-\ln T) &= \frac{2}{\Delta E^2}\,. \end{aligned} \tag{14.4}$$

Fig. 14.3 repeats the plot of $T(E)$ versus E shown in Fig. 14.2, shows $-\ln T(E)$ versus E (looks like a parabola) and shows a plot of the first derivative of this function. The first derivative is definitely not a straight line. Therefore we can reject the guess that the resonance has a Gaussian form.

Lorentzian. If the curve shown in Fig. 14.2 is a Lorentzian, it has the form

$$T(E) = \frac{A}{1 + \left(\frac{E - E_0}{\Delta E}\right)^2}\,, \tag{14.5}$$

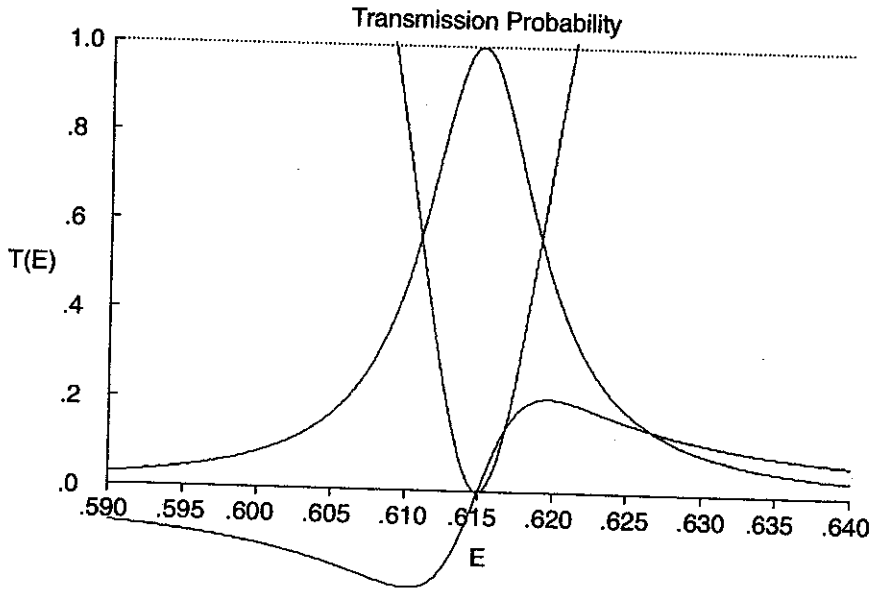

Fig. 14.3 Negative logarithm of the transmission peak (parabola-shaped curve) superposed on the peak. If the peak is a Gaussian, the derivative of its negative logarithm will be a straight line. The derivative is not even close to a straight line, so the peak is not approximated by a Gaussian function.

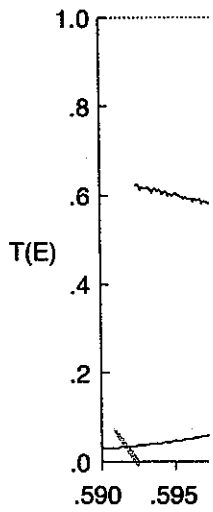

Fig. 14.4 Reciprocal
peak. If the peak is a L
positive slope and the s
proximated by a straight
does not vary "too muc
approximated by a Lore
half height) 0.0046 eV.

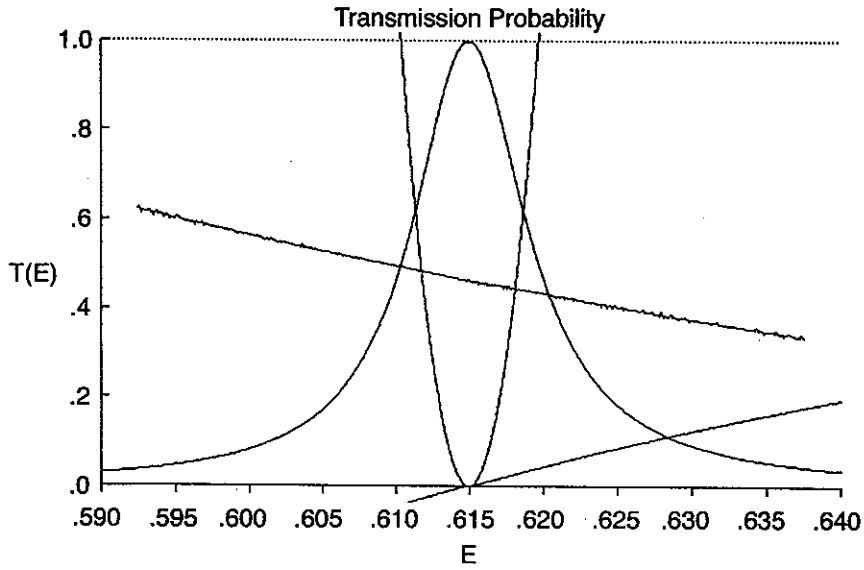

Fig. 14.4 Reciprocal of the transmission peak (parabola-shaped curve) superposed on the peak. If the peak is a Lorentzian, the derivative of the reciprocal will be a straight line with positive slope and the second derivative will be a constant. The first derivative is well approximated by a straight line with positive slope. The second derivative (with negative slope) does not vary "too much" through this resonance. This shows the resonance curve is well approximated by a Lorentzian function with energy maximum at 0.6150 eV and half width (at half height) 0.0046 eV.

where E_0 is the location of the peak and ΔE is the half width at half height. By taking the reciprocal we should find a rising parabola

$$\frac{1}{T(E)} = \frac{1}{A} + \frac{1}{A}\left(\frac{E - E_0}{\Delta E}\right)^2 . \tag{14.6}$$

Once again, the first derivative should be a linear function of E with positive slope, and the second derivative should be a constant. In Fig. 14.4 we show the resonance, with its reciprocal -1 (since $A = 1$), the first, and the second derivative. These plots are superposed on the original resonance curve. The first derivative (positive slope) is computed by first differencing the data; the second derivative (negative slope) is the first difference of the first derivative (i.e., second difference). The scales of these derivatives have been adjusted so the properties of the curves are evident. The second derivative decreases somewhat with increasing energy. This is an effect of the peaks at higher energies.

The results of Figs. 14.3 and 14.4 clearly distinguish between the Gaussian and Lorentzian line shapes. We conclude that the lowest resonance shown in Fig. 14.1 and enlarged in Fig. 14.2 is Lorentzian in shape, with peak at $E = 0.6150$ eV and half width $\Delta E = 0.0046$ eV.

Problem. Fix V, D, the height and width of the two identical potential barriers (for example, $V = 20$ eV, $D = 2$ Å). Vary L, the distance between the two potential barriers, and try to determine the dependence of the centers of the lowest peaks on L. You might infer from the data that $E_c(n)$, the center of the nth peak, is inversely proportional to L^2. Plot $E_c(n)L^2$ as a function of L to check this guess. You might also guess that the center of the nth peak behaves like n^2. To test this guess, plot $E_c(n)L^2/n^2$ versus L for the lowest peaks in the transmission probability spectrum. The results are shown in Fig. 14.5. This figure shows: the double barrier; the energies at which the transmission peaks occur for $E < V = 20$ eV, plotted as a function of L; and the ratio of the transmission peak energies, $E/E(n, L)$, plotted as a function of L, where $E(n, L) = (\hbar^2/2m)(n\pi/L)^2$.

Problem. Fix L and V, and vary D (for example, $V = 20$ eV and $L = 4$ Å). You might expect the half widths of the Lorentzian peaks to decrease exponentially with the width D of the classically forbidden region: $\Delta E \sim e^{-\lambda D}$. To test this hypothesis, plot $-\ln(\Delta E)/D$ as a function of D for the lowest transmission resonance peaks. In fact, you might even guess that $-\ln(\Delta E) \sim \int \kappa(x)\, dx$, where the integral extends through (both) classically forbidden regions. To test this guess, plot $-\ln(\Delta E)/(2D\sqrt{2m(V - E_{\text{peak}})/\hbar^2})$ as a function of D for the lowest peaks in the transmission spectrum. The results are shown in Fig. 14.6. This figure shows: the double barrier ($V = 20$ eV and $L = 4$ Å); the natural logarithm of the full width at half height of the Lorentzian peak plotted as a function of D, the width of either barrier; and the ratio of this logarithm to the action, $-\ln(\Delta E)/A$, plotted as a function of D, where $A = 2D\sqrt{2m(V - E_{\text{peak}})/\hbar^2}$.

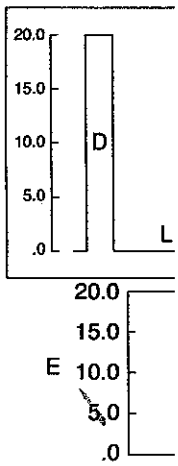

Fig. 14.5 Plot of E
$(\hbar^2/2m)(n\pi/L)^2$. T
Å, but their separatior
varies from three at L
value suggests that for
$E_n \simeq (\hbar^2/2m)(n\pi/$

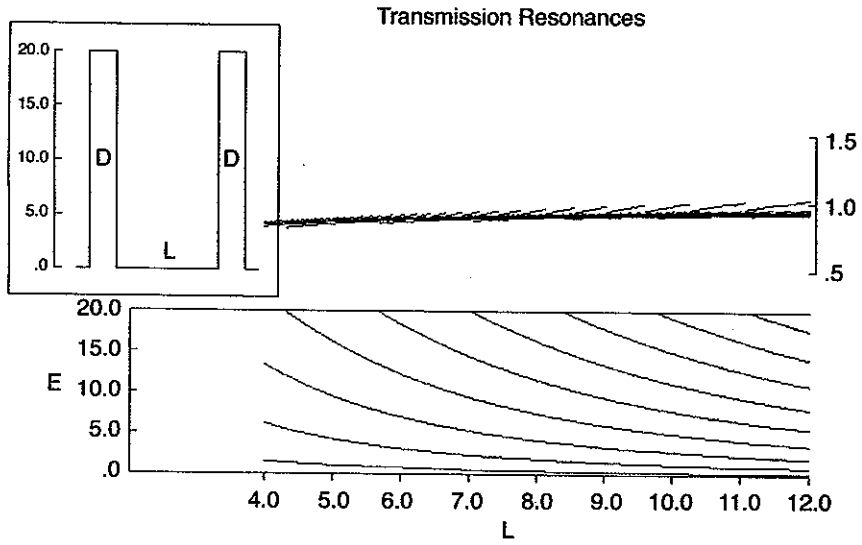

Fig. 14.5 Plot of $E_n/E(n,L)$ vs. L for the double barrier potential, where $E(n,L) = (\hbar^2/2m)(n\pi/L)^2$. The two identical barriers have constant height 20 eV and thickness 2 Å, but their separation, L, varies from 4 Å to 12 Å. The number of resonances below 20 eV varies from three at L = 4 Å to nine at 12 Å. The approach of all scaled energies to a common value suggests that for the "deep" resonances ($\kappa L/\hbar \geq 1$) the energies of the resonances are $E_n \simeq (\hbar^2/2m)(n\pi/L)^2$.

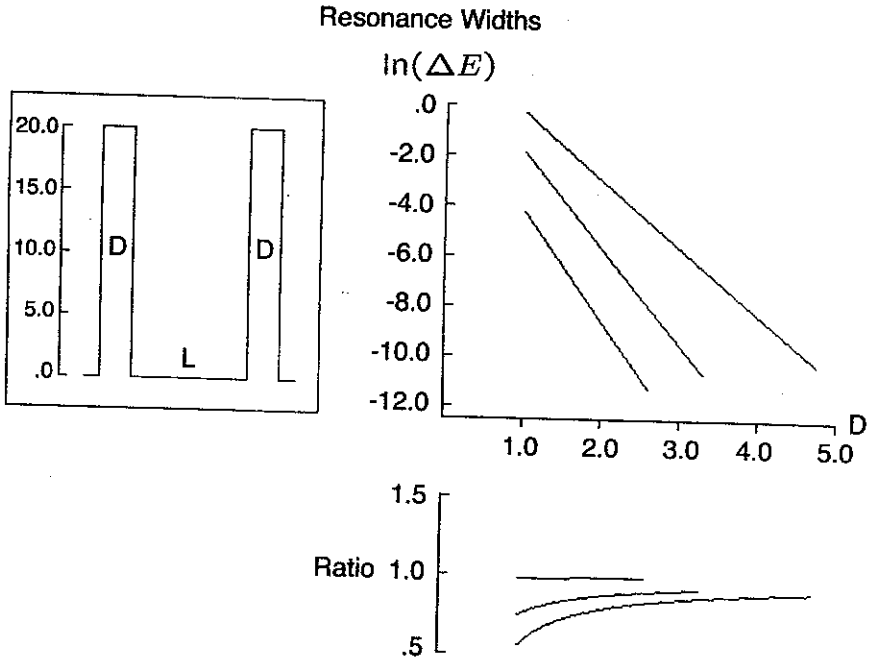

Fig. 14.6 Plot of $-\ln(\Delta E)$ as a function of D for the double barrier potential, where ΔE are the full widths at half height of each of the three resonance peaks that exist for this double barrier potential. The two identical barriers have constant height 20 eV and separation 4 Å, but their thickness, D, varies from 1.0 Å to 5.0 Å. *Below*, Plot of the ratio $-\ln(\Delta E)/2\kappa D$ as a function of D, where $\kappa = \sqrt{2m(V - E_{\text{peak}})/\hbar^2}$. The approach of all scaled ratios to a common value suggests that the linewidth of the "deep" resonances decreases exponentially: $\Delta E \simeq \exp\left[-2D\sqrt{2m(V - E_{\text{peak}})/\hbar^2}\right]$.

If a second barrier b
spectrum (see Fig. 1
To explore this c
rectangular barriers,
other by a distance i
$T(E)$ versus E, is t
splits into a doublet
The transmission
above but with one
split into a triplet of
This behavior is
separated by equal

1. Each peak sp
2. The "center o
the correspon
3. The width of
small values c
barrier spectr
at least for cl

It is possible to d
we delay answering
(Part IV).

15

Multiple Barriers

If a second barrier behind the first produces surprises in the transmission probability spectrum (see Fig. 14.1), what will a third behind the second do?

To explore this question we computed $T(E)$ for a potential consisting of three rectangular barriers, each of height V eV and width D Å, and separated from each other by a distance L Å (Fig. 15.1). The principal effect, clearly visible in the plot of $T(E)$ versus E, is that each peak in the transmission spectrum of the double barrier splits into a doublet in the transmission spectrum for the triple barrier.

The transmission probability spectrum for a quadruple barrier, formed as described above but with one more rectangular barrier, is shown in Fig. 15.2. Each peak is now split into a triplet of peaks.

This behavior is systematic. For a potential consisting of $N + 1$ identical barriers separated by equal distances, we find

1. Each peak splits into an N-tuplet.
2. The "center of gravity" of each N-tuplet occurs at roughly the same energy as the corresponding peak in the transmission spectrum of the double barrier.
3. The width of each multiplet grows slowly with N, and saturates for relatively small values of N. That is, the N-tuplet corresponding to one peak of the double barrier spectrum does not overlap the N-tuplet corresponding to another peak, at least for classically forbidden energies.

It is possible to determine how the width of each N-tuplet saturates as $N \to \infty$, but we delay answering this question until we discuss energy bands for periodic lattices (Part IV).

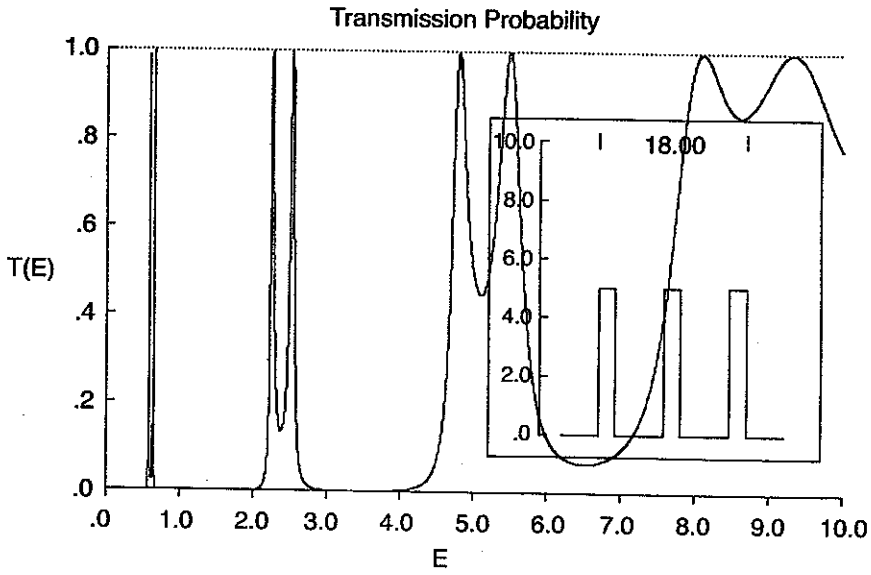

Fig. 15.1 Transmission probability spectrum for three identical barriers with $V = 5$ eV, $D = 2$ Å, and $L = 6$ Å. Each peak is a doublet.

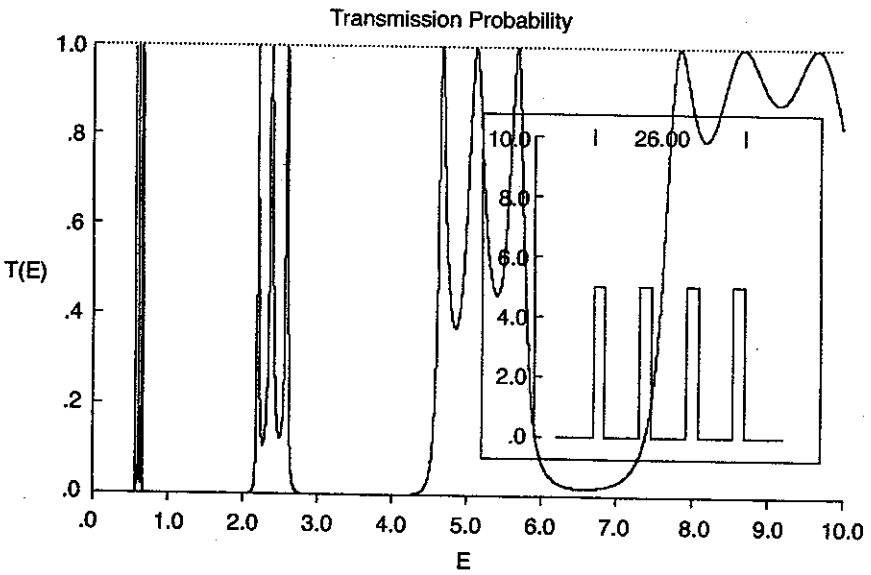

Fig. 15.2 Transmission probability spectrum for four identical barriers separating three identical wells. As in Fig. 15.1, $V = 5$ eV, $D = 2$ Å, and $L = 6$ Å. Each peak is a triplet.

Pro

In order to determin
trum of the double ba
as it is scattered fror

The problem has

computed the transfe

$\begin{bmatrix} A \\ B \end{bmatrix}_{j+1}$ in regior

possible to reduce t
probability density.

To do this, we cl
regions of constant p

$$E > V$$
$$E = V$$
$$E < V$$

In addition, within e
$(0 \leq x_j \leq \delta_j$ for x_j
first derivative at the
of the form

$$\begin{bmatrix} \cos\ k_j\delta_j \\ -k_j \sin\ k_j\delta_j \end{bmatrix}$$

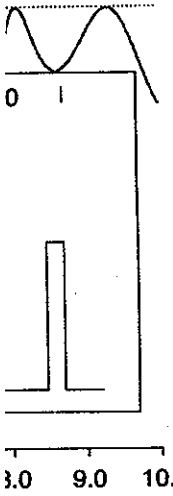

arriers with $V = 5$ eV,

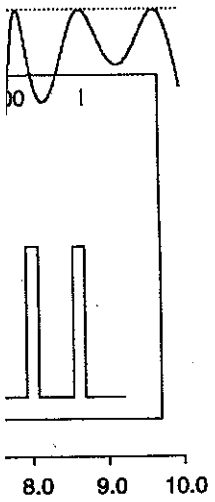

barriers separating three
Å. Each peak is a triplet.

16

Probability Distributions

In order to determine why there are resonances in the transmission probability spectrum of the double barrier, it is useful to compute the probability density of the electron as it is scattered from this potential.

The problem has been solved in principle in Part I, chapter 3. In that chapter we computed the transfer matrix relating amplitudes $\begin{bmatrix} A \\ B \end{bmatrix}_j$ in region j to the amplitudes $\begin{bmatrix} A \\ B \end{bmatrix}_{j+1}$ in region $j+1$. These 2×2 transfer matrices (3.7) are complex. It is possible to reduce the number of complex operations involved in computing the probability density.

To do this, we choose a different set of solutions to Schrödinger's equation in regions of constant potential:

$$\begin{array}{lcll} & \Phi_1(x) & \Phi_2(x) & \\ E > V & \cos kx & \sin kx & k = \sqrt{2m(E-V)/\hbar^2} \\ E = V & 1 & x & \\ E < V & \cosh \kappa x & \sinh \kappa x & \kappa = \sqrt{2m(V-E)/\hbar^2}\,. \end{array} \tag{16.1}$$

In addition, within each region we measure distance from the left edge to the right ($0 \le x_j \le \delta_j$ for x_j in region j). Imposing continuity of the wavefunction and its first derivative at the boundary between region j and region $j+1$ leads to an equation of the form

$$\begin{bmatrix} \cos\, k_j\delta_j & \sin\, k_j\delta_j \\ -k_j \sin\, k_j\delta_j & k_j \cos\, k_j\delta_j \end{bmatrix} \begin{bmatrix} A \\ B \end{bmatrix}_j = \begin{bmatrix} 1 & 0 \\ 0 & k_{j+1} \end{bmatrix} \begin{bmatrix} A \\ B \end{bmatrix}_{j+1} \tag{16.2}$$

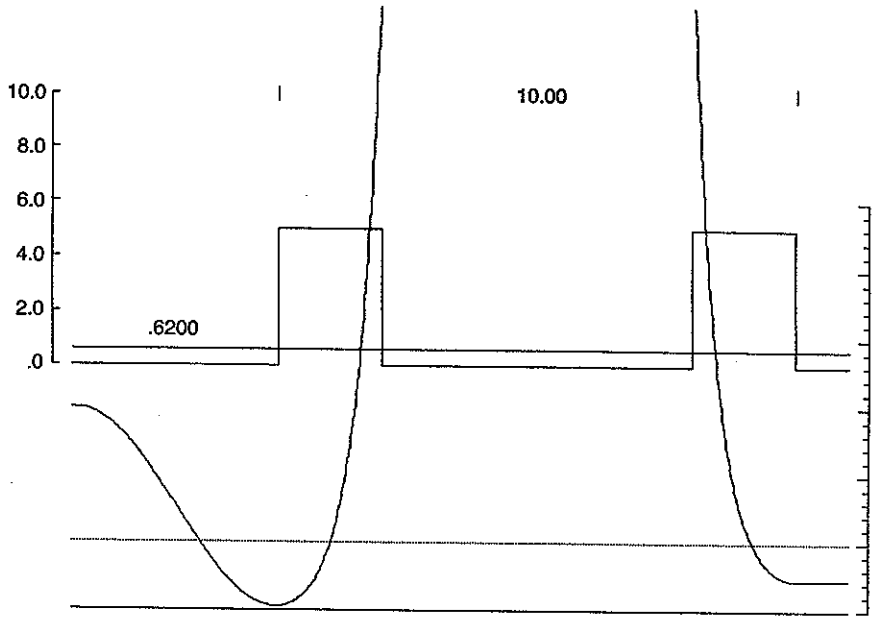

Fig. 16.1 Probability density for an electron of energy $E = 0.62$ eV incident on the double barrier shown in Fig. 14.1. The energy chosen sits on the shoulder just above the peak, at about $T(E) = 0.6$ (see Fig. 14.2). Closer to the peak, the probability density between the barriers becomes much larger.

in the case $E > V_j, E > V_{j+1}$. Analogous equations apply for all conditions (i.e., $E > V_j, E < V_{j+1}$, etc.). All 2×2 transfer matrices involved in propagating the amplitudes $\begin{bmatrix} A \\ B \end{bmatrix}_{j+1}$ to the amplitudes $\begin{bmatrix} A \\ B \end{bmatrix}_j$ in the adjacent region are now real. Only the amplitudes themselves are complex.

This set of equations for the amplitudes is initialized by setting

$$\begin{aligned} \Phi_R(x) &= \sqrt{T}\, e^{ik_R x} = \sqrt{T}\,(\cos\, k_R x + i\, \sin\, k_R x)\,, \\ \begin{bmatrix} A \\ B \end{bmatrix}_R &= \sqrt{T} \begin{bmatrix} 1 \\ i \end{bmatrix}. \end{aligned} \tag{16.3}$$

Using this procedure, we have computed the probability density $|\Phi(x;E)|^2$ for a particle of energy E scattered by the double well potential shown in Fig. 14.1. These probability densities are computed for energies near the maxima ($E = 0.62$ eV, $E = 2.31$ eV) of the lowest two peaks, and are shown in Figs. 16.1 and 16.2.

The results of these computations can be summarized in the following observations, some of which are apparent from the figures.

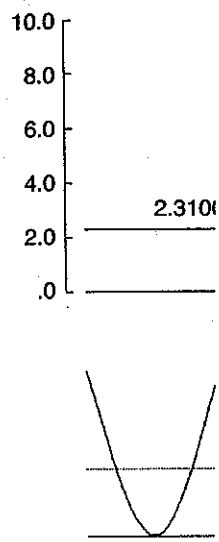

Fig. 16.2 Probability
The energy ($E = 2.31$
probability is about 0.2

1. The probabilit
the boundary c

2. The probabili
from the boun
$\overline{R}R + (Re^{-2ik}$
by k_L ($\lambda = \pi$
edge of the sc
in the left-han
right-hand reg

3. The probabili
ratio of the m
intensity varie
resonance pea

4. Near the lowe
has a single r
$T(E)$, the pr
by a node tha

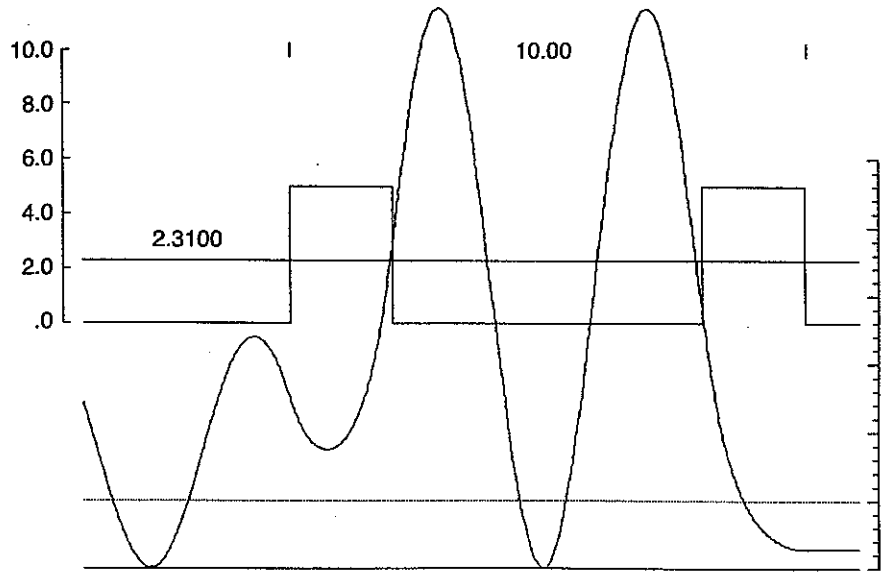

Fig. 16.2 Probability density for an electron in the double barrier potential shown in Fig. 14.1. The energy ($E = 2.31$ eV) is just below the second peak. At this energy, the transmission probability is about 0.28.

1. The probability density in the right-hand region is constant. This follows from the boundary condition that is imposed: $\Phi_R(x) = \sqrt{T}\, e^{+ik_R x}$, $|\Phi_R(x)|^2 = T$.

2. The probability density oscillates in the left-hand region. This also follows from the boundary condition: $\Phi_L(x) = e^{+ik_L x} + Re^{-ik_L x}$, $|\Phi_L(x)|^2 = 1 + \overline{R}R + (Re^{-2ik_L x} + \overline{R}e^{+2ik_L x})$. The wavelength of the oscillation is determined by k_L ($\lambda = \pi/k_L$); the phase of R determines the probability at the left-hand edge of the scattering potential. If $R = 0$ (i.e., $T = 1$), the probability density in the left-hand region is also constant and equal to the constant value in the right-hand region if $V_L = V_R$.

3. The probability density between the double barriers can be very high. The ratio of the maximum probability density between the barriers to the incident intensity varies as the energy is swept and assumes a maximum value at the resonance peaks.

4. Near the lowest peak of the transmission spectrum $T(E)$ the probability density has a single maximum. Near the second peak in the transmission spectrum $T(E)$, the probability density exhibits two peaks. These peaks are separated by a node that approaches zero quadratically.

5. The probability density associated with the nth peak in the spectrum of $T(E)$ shows n peaks. These are separated by $n-1$ nodes that approach zero quadratically.

6. Peaks in the transmission spectrum occur at energies for which particles exhibit constructive interference. That is, when a particle inside the double barrier starts at the right-hand edge of the barrier on the left and travels to the left-hand edge of the barrier on the right, it undergoes a phase shift $\int_a^b p\ dx/\hbar = kL$. On reflecting off the right-hand barrier, it undergoes a phase shift of approximately π (the larger $\sqrt{2m(V-E)/\hbar^2}\ D$, the closer to π). On traveling to the left-hand well and reflecting off it, the particle undergoes another equal phase shift of about $kL+\pi$. If the total phase shift in this round trip is an integer multiple of 2π, the particle will interfere with itself constructively. Therefore, resonances occur for $2kL + 2\pi \sim 2\pi n$, or energies given by

$$E_n \sim \frac{\hbar^2}{2m}\left(\frac{n\pi}{L}\right)^2. \tag{16.4}$$

This approximation is valid when $\sqrt{2m(V-E)/\hbar^2}\ D$ is large.

The probability densities for triple, quadruple, and so forth, barrier potentials have also been computed. For a triple barrier, each peak in the transmission spectrum is a doublet (see Fig. 15.1). The probability densities for energies corresponding to the two peaks in a doublet are very similar. We will not learn what the difference between the corresponding scattering states is by studying probability densities. Rather, we must study the appropriate wavefunctions. This study will be left to Part III, chapter 29.

In the previous cha
chanical tunneling t
double (and multipl
in the transmission
We now ask wh
end, we study the tr
Å), B (4.0 eV, 2.0 Å
$V = 0$ eV, while ba
Before studying
probability spectrur
plots contain no su
double barrier AB
4.0 eV. These three
eV does not appea
limitations. A peak
peak has a maximu
The spectrum of
maximum occurs i
about 1.3 eV. A se
4.5 eV, but at this r
The transmissio
spectrum exhibits
eV is invisible due

17

Combining Barriers

In the previous chapters, we have developed some understanding of quantum mechanical tunneling through a single barrier. We have also studied tunneling through double (and multiple identical) barriers and have understood the occurrence of peaks in the transmission probability spectrum as a resonance phenomenon.

We now ask what happens when we combine several different barriers. To this end, we study the triple barrier system consisting of barriers A ($V = 5.0$ eV, $\delta = 1.5$ Å), B (4.0 eV, 2.0 Å), and C (3.0 eV, 2.5 Å). Barriers A and B are separated by 7 Å at $V = 0$ eV, while barriers B and C are separated by 3 Å, also at $V = 0$ eV.

Before studying this set of three barriers, we study separately the transmission probability spectrum for the double barriers AB (Fig. 17.1) and BC (Fig. 17.2). These plots contain no surprises. Peaks occur in the classically forbidden regime. For the double barrier AB (Fig. 17.1) these peaks occur at energies of about 0.4, 1.9, and 4.0 eV. These three peaks have maxima at $T(E) = 1.0$; the very narrow peak at 0.4 eV does not appear to have maximum at $T(E) = 1.0$ only because of resolution limitations. A peak occurs in the scattering region $[E > \min(A, B) = 4.0]$, but this peak has a maximum transmission probability $T(E) < 1$.

The spectrum of $T(E)$ for the double barrier BC exhibits similar properties. One maximum occurs in the classically forbidden region $[E < \min(B, C) = 3.0$ eV] at about 1.3 eV. A second maximum occurs in the classically allowed region at about 4.5 eV, but at this maximum $T(E) < 1$.

The transmission probability for the triple barrier ABC is shown in Fig. 17.3. This spectrum exhibits peaks at about 0.4, 1.3, 1.9, 3.9, 4.6, and 7.0 eV. The peak at 0.4 eV is invisible due to resolution limits. In this figure we observe two things:

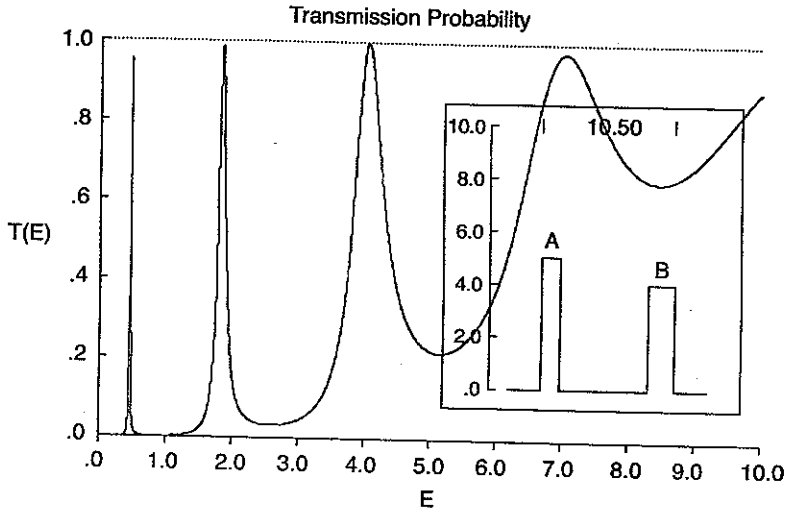

Fig. 17.1 Transmission spectrum of the double barrier AB. Transmission peaks occur in the classically forbidden regime at ~ 0.4, 1.9, and 3.9 eV. These have maxima at $T(E) = +1$, although they are resolution limited in this plot. The peak at 7.0 eV in the classically allowed regime has maximum at $T(E) < +1$. Inset provides information on the height and total length of the barrier.

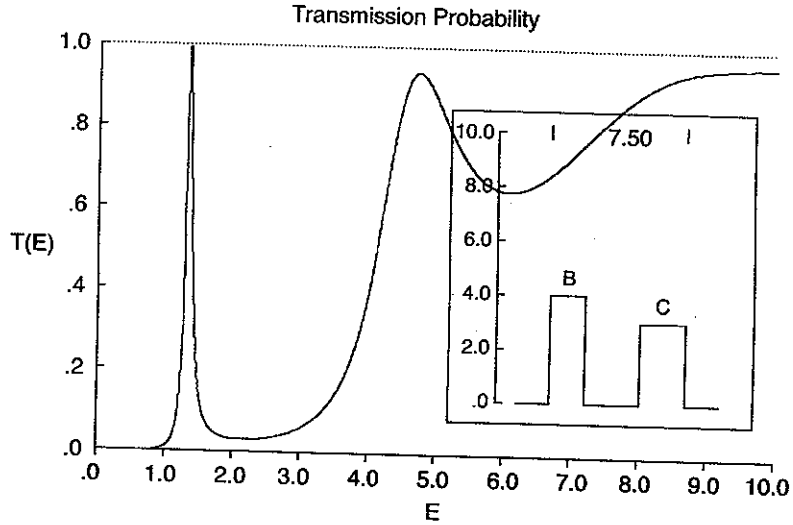

Fig. 17.2 Transmission spectrum of the double barrier BC. Transmission peaks at 4.5 and 10^+ eV in the classically allowed regime have maxima below $T(E) = +1$.

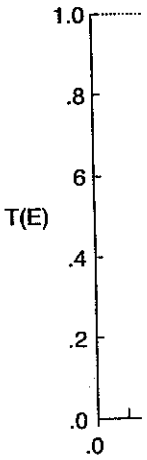

Fig. 17.3 Transmis
and C = (3.0, 2.5) (e
at 0.4, 1.9, 3.9, and 7.
4.9 eV are due to reso

1. The peaks at
AB (see Fig.
double barrie

2. None of the p

We can check th
in Fig. 17.3 actuall
densities for energ
potential have been
and $E = 7.0$ eV (F
Fig. 17.4 (E =
larger between wel
to a resonance bet
resonate in the BC
transmission reson
The probability
in the BC well has
peak in the BC dou
below 0.4 eV in the
are so narrow that
Fig. 17.5 (E =
between barriers A

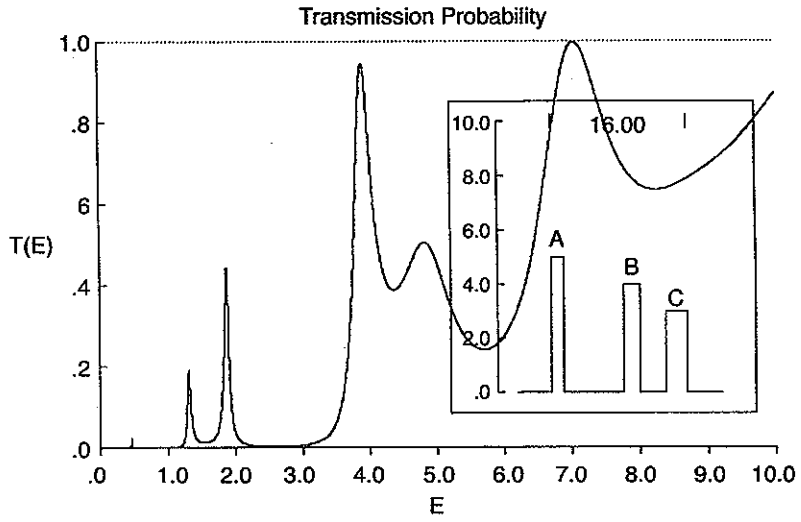

Fig. 17.3 Transmission spectrum of the double barrier ABC, A = (5.0, 1.5), B = (4.0, 2.0), and C = (3.0, 2.5) (eV, Å). Barriers A and B are separated by 7.0 Å, B and C by 3 Å. Peaks at 0.4, 1.9, 3.9, and 7.0 eV arise from resonances in the AB double barrier, those near 1.3 and 4.9 eV are due to resonances in the BC double barrier.

1. The peaks at 0.4, 1.9, 3.9, and 7.0 eV seem to be related to the double barrier AB (see Fig. 17.1), while the peaks at 1.3 and 4.6 eV seem to be related to the double barrier BC (see Fig. 17.2).

2. None of the peaks has a maximum value of +1.

We can check that the fingerprints we have used to identify the peaks that appear in Fig. 17.3 actually lead to correct identifications by computing relative probability densities for energies near these peaks. Probability densities in the triple barrier potential have been computed for $E = 1.31$ eV (Fig. 17.4), $E = 3.65$ eV (Fig. 17.5), and $E = 7.0$ eV (Fig. 17.6).

Fig. 17.4 ($E = 1.31$ eV) shows that the electron probability density is much larger between wells B and C than between A and B. This peak is therefore due to a resonance between wells B and C. Since an electron with energy matched to resonate in the BC well will not be in resonance in the AB well, the maximum of the transmission resonance peak near 1.3 eV is less than +1.

The probability distribution in Fig. 17.4 tells us more. Since the probability density in the BC well has no nodes, this peak corresponds to the lowest energy transmission peak in the BC double well potential. In particular, this means that there are no peaks below 0.4 eV in the transmission spectrum of the BC double barrier (Fig. 17.2), which are so narrow that they are not even hinted at in the transmission spectrum.

Fig. 17.5 ($E = 3.65$ eV) shows that the electron probability density in the well between barriers A and B is much larger than between barriers B and C. Thus the

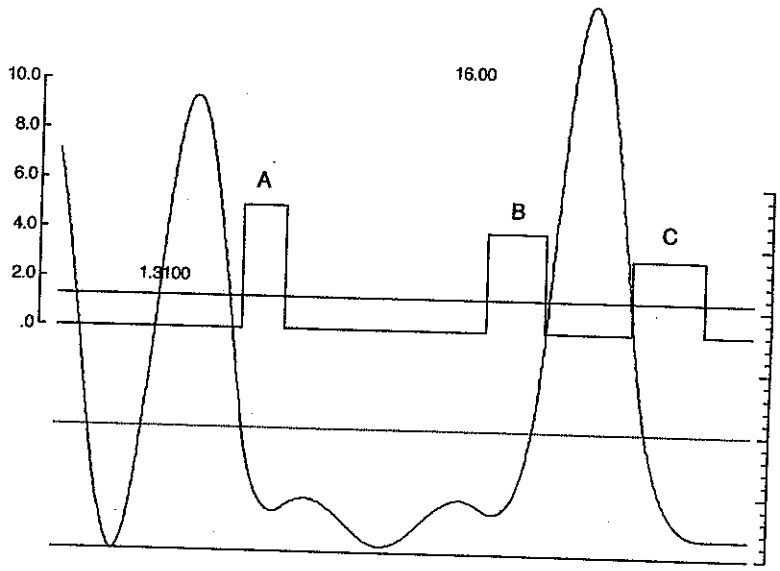

Fig. 17.4 *Above*, Triple well potential with energy scale at left. *Below*, Probability density for electron with energy $E = 1.31$ eV. *Dotted*, Probability density $= +1$ (scale at right). The resonance peak near 1.3 eV is due to the lowest resonance in the BC double barrier.

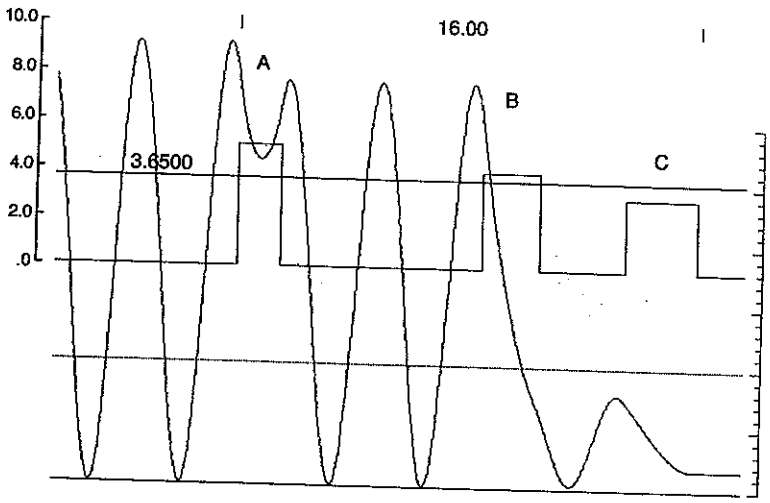

Fig. 17.5 *Above*, Triple well potential with energy scale at left. *Below*, Probability density for electron with energy $E = 3.65$ eV. *Dotted*, Probability density $= +1$ (scale at right). The resonance peak near 3.9 eV is due to the third resonance in the AB double barrier. The wavefunction has two nodes in the AB double barrier, but since the minimum probability density in the BC double barrier is not zero, the wavefunction has no nodes in this region.

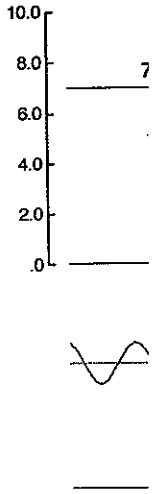

Fig. 17.6 *Above*, T
for electron with ene
resonance peak near
probability density f
wavefunction has no

peak at 3.9 eV is p
resonance? Since
the peak is the thi
the AB double bar

The presence c
between one and t
to resonances in t
whether this numb

Fig. 17.6 ($E =$
barriers A and B
the cavity betwee
in this region, it c
We observe that t
means the wavefu
barrier. This is cl
classically allowe

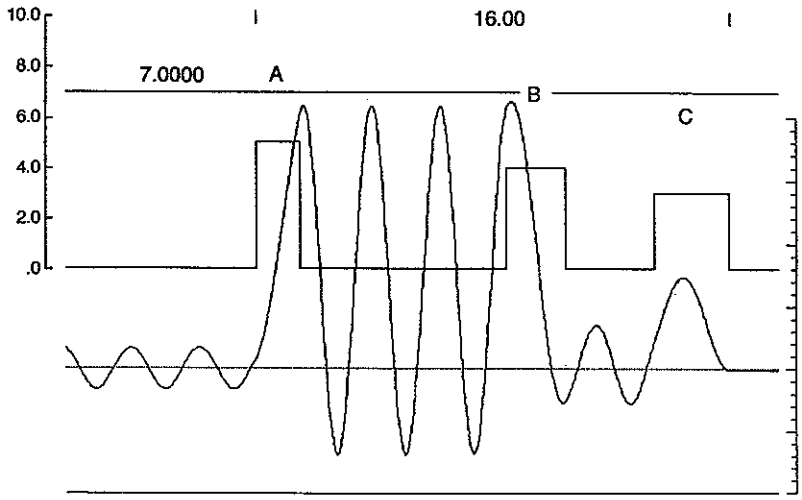

Fig. 17.6 *Above*, Triple well potential with energy scale at left. *Below*, Probability density for electron with energy $E = 7.0$ eV. *Dotted*, Probability density $= +1$ (scale at right). The resonance peak near 7.0 eV is due to the fourth resonance in the AB double barrier. The probability density for this classically allowed energy has minima that are nonzero, so the wavefunction has no nodes in this potential.

peak at 3.9 eV is primarily due to a resonance in the region between A and B. Which resonance? Since the probability density exhibits two nodes in this region of space, the peak is the third resonance (transmission peak) in the transmission spectrum of the AB double barrier.

The presence of one node between barriers B and C means that, at this energy between one and three [(1+1) ±1] resonance peaks in the spectrum have occured due to resonances in the BC cavity. The location of the node can be used to determine whether this number is one, two, or three. We will not discuss this point now.

Fig. 17.6 ($E = 7.0$ eV) shows the electron probability density is larger between barriers A and B than between B and C. Thus, this peak is due to a resonance in the cavity between barriers A and B. Since the probability density has three minima in this region, it corresponds to the fourth transmission resonance of the AB cavity. We observe that the probability distribution has minima that do not reach zero. This means the wavefunction is not zero (there are no nodes) anywhere in this multiple barrier. This is characteristic of wavefunctions for electrons with energies in the classically allowed regime.

18

Quantum Engineering

As the size of electronic devices shrinks, the laws of quantum mechanics play an increasingly important role in their behavior. It should be possible to use these laws to design devices to operate within preset design specifications.

We illustrate this process with a simple example. Suppose electrons are conveniently available in some particular range of energies (e.g., 0-2 eV), but we need electrons in a much smaller energy range (e.g., 1 ± 0.2 eV). Can we design a filter that will pass electrons in this restricted range and reject electrons outside this range? How?

The specifications just described can be expressed as conditions on the transmission probability function $T(E)$: it is zero in the interval from 0 to 2 eV, except in the smaller interval around 1 eV from $1 - 0.2$ to $1 + 0.2$ eV. Our experience with transmission probability coefficients is

1. A single rectangular barrier will not exhibit resonance structures in the classically forbidden region.
2. A double barrier will exhibit resonance peaks at which 100% transmission is achieved.
3. Multiple different barriers will show resonance structure, but transmission peaks do not rise to $+1$.
4. Multiple identical equally spaced barriers produce multiplets of transmission peaks showing 100% transmission.

These observations suggest that a filter with the specified characteristics can be produced by fabricating a device with a large number of identical equally spaced

barriers. If the barriers are rectangular, the multiple barrier device is specified by four parameters: $N+1$, the number of barriers; V (eV), the height of each; D (Å), the width of each; and L (Å) the spacing between adjacent barriers.

A useful approach is to design a double barrier so that one of the resonance peaks falls more or less in the middle of the range of energies to be transmitted, while all other resonances fall outside this range. For the design characteristics specified, we will search for parameters L, D, V for which the lowest transmission peak is ~ 1 eV and the higher energy peaks occur for energies greater than 2 eV. The location of the transmission peaks depends more sensitively on L than D or V. We can use the (Action) resonance condition for round trips in the double barrier potential

$$2pL/\hbar + \text{phase shifts at 2 boundaries} = 2\pi n$$

to estimate L. The argument is that each reflection phase shift is $\sim \pi$, so that $2L\sqrt{2mE}/\hbar \sim 2\pi n$ or $L \sim n\pi/\sqrt{2mE/\hbar^2} \sim 6$ Å for $E = 1$ eV, $n = 1$. This quick and dirty estimate at least puts us in the right ballpark for a more refined estimation of the design parameters. After a few computations, we find that design parameters $L = 4.0$ Å, $D = 1.0$ Å, $V = 3.8$ eV produce a transmission probability spectrum, shown in Fig. 18.1, with the desired characteristics. That is, the lowest resonance occurs at about 1 eV and the next resonance is well above 2 eV.

In Fig. 18.2 we present the spectrum of $T(E)$ for a six-barrier device with five potential wells between the six barriers. Each peak from the double barrier potential is now a 5-plet. In each multiplet the maximum value of $T(E)$ is $+1$ and the minimum rises towards the center of the transmission band.

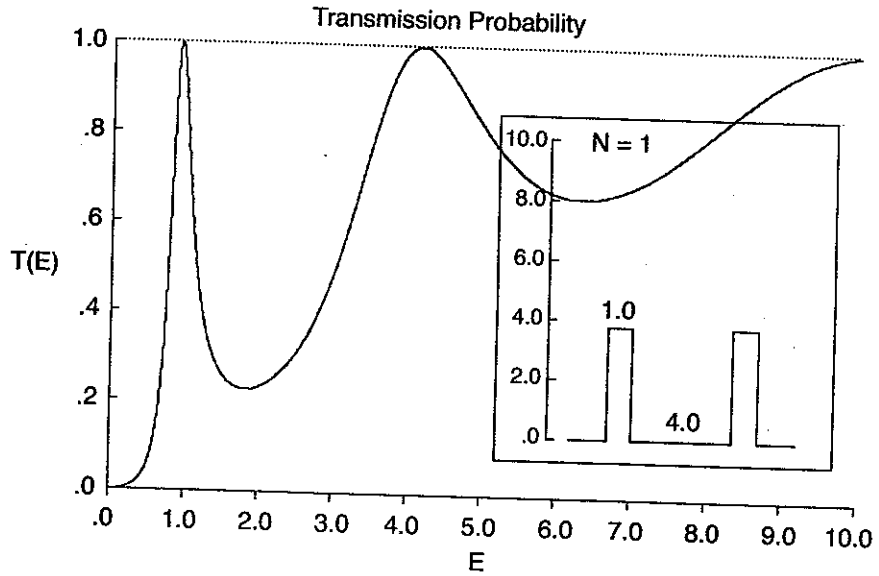

Fig. 18.1 Double barrier designed to have one peak at about 1.0 eV. *Inset*, Barrier height $V = 3.8$ eV, width $D = 1.0$ Å, separation between barriers $L = 4.0$ Å. There is one ($N = 1$) well between the two barriers.

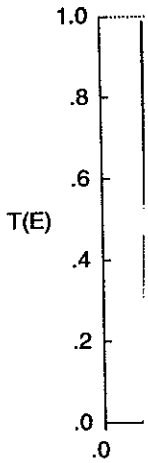

Fig. 18.2 Transmis
by $N+1$ barriers. N

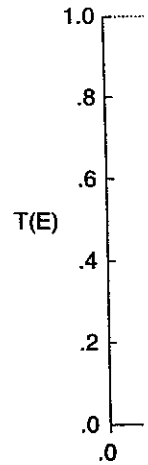

Fig. 18.3 Transmi
number of barriers (ν
probability between

ice is specified by four
ht of each; D (Å), the
's.
of the resonance peaks
transmitted, while all
teristics specified, we
smission peak is ~ 1
2 eV. The location of
or V. We can use the
rier potential

$2\pi n$

hift is $\sim \pi$, so that
$E = 1$ eV, $n = 1$.
ark for a more refined
s, we find that design
nsmission probability
s. That is, the lowest
above 2 eV.
rrier device with five
ouble barrier potential
$+1$ and the minimum

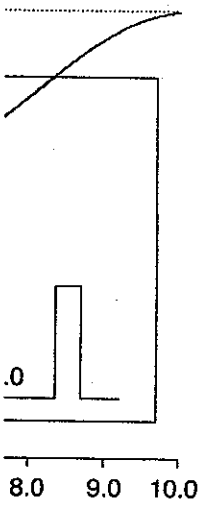

V. *Inset*, Barrier height
. There is one ($N = 1$)

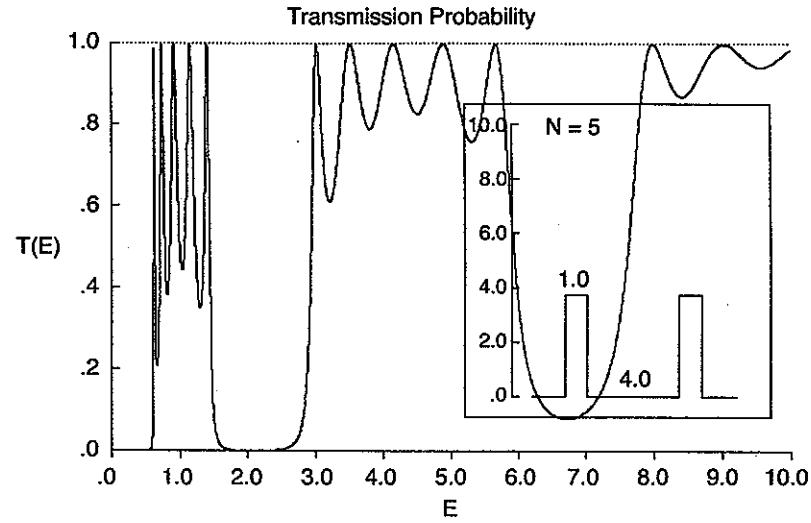

Fig. 18.2 Transmission probability spectrum of multiple barrier with N (= 5) wells formed by $N + 1$ barriers. N is given in the inset.

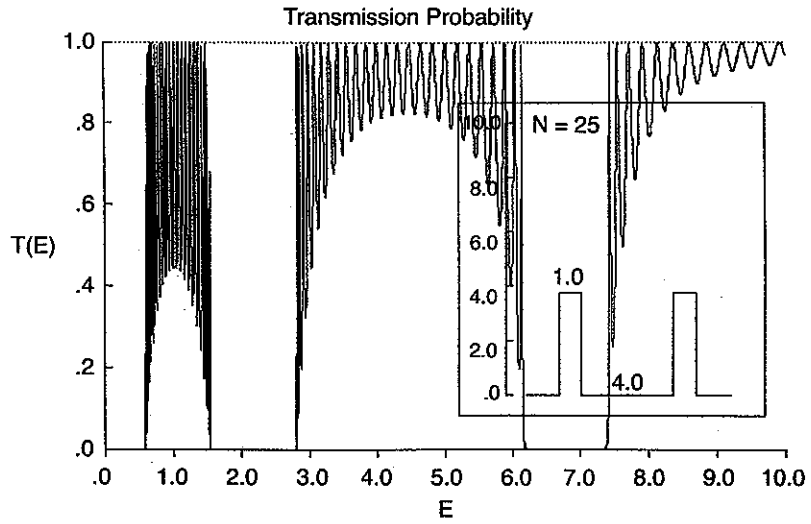

Fig. 18.3 Transmission probability spectrum of multiple barrier with $N = 25$. As the number of barriers (wells) increases, the pass bands approach $T(E) \simeq 1$ and the transmission probability between these bands approaches zero ("forbidden bands").

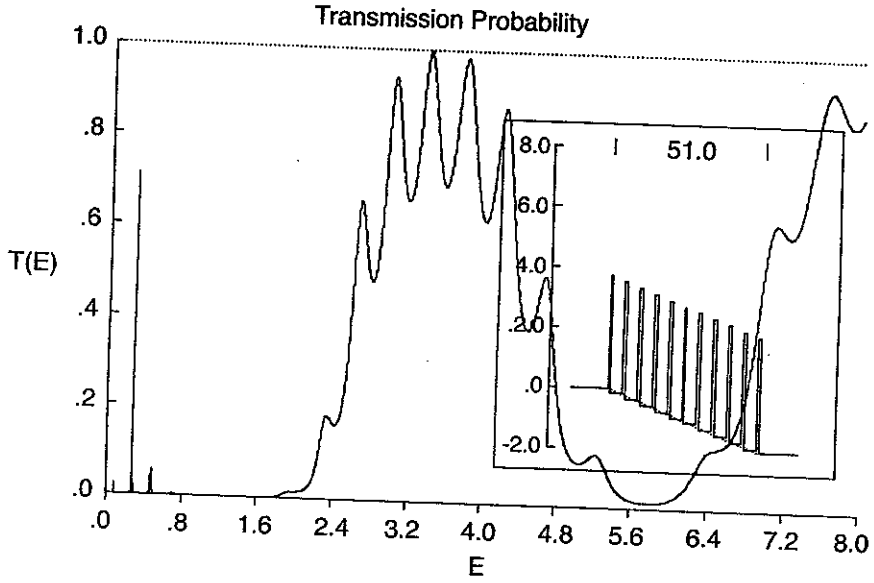

Fig. 18.4 Transmission probability spectrum for multiple barrier ($N = 10$) biased by a 2-V external electric field. The field displaces and distorts the transmission probability spectrum.

One way to smooth the transmission spectrum within each band is to crowd more peaks into this range. This is easily done by building more barriers. It is surprising, but true, that the width of each band is almost independent of N for N sufficiently large ($N \geq 5$). The width of these bands is strongly determined by D and V, more specifically by $D\sqrt{V - E_{Res}}$. We present the transmission spectrum of a device with $N = 25$ (26 barriers) in Fig. 18.3. Notice that the widths of the transmission pass bands are almost unchanged from the $N = 5$ to the $N = 25$ device.

The transmission properties of a multiple barrier potential can be altered by biasing it. That is, we impose an electric field on the device by creating a potential difference across it. In Fig. 18.4 we show (inset) an eleven-barrier potential with a 2-V bias. That is, the left-hand edge is grounded ("grounded" means the potential is zero), while the right-hand edge is held at +2 V. Since the electron charge is negative, the potential of the electron at the right-hand edge is -2 eV. We assume a linear decrease of potential between the left- and right-hand edges and approximate the barrier potential in the region as before. That is, we assume the potential in each of the $2N + 1$ regions is a constant whose value is the value of the potential at the midpoint of the region. Biasing in this way modifies the structure of the pass bands and pulls them to lower energy. If we assume that the electrons that are available to transit this barrier from left to right are thermal (i.e., energies $\leq 1/40$ eV at room temperature), then we can compute the transmission probability, and the conductance, of this device as a function of the bias voltage. The conductance function will not be a monotonic function of V and will therefore show regions of negative resistivity. A more complete discussion of this phenomenon is outside the scope of our subject, which is *elementary* quantum mechanics in one dimension.

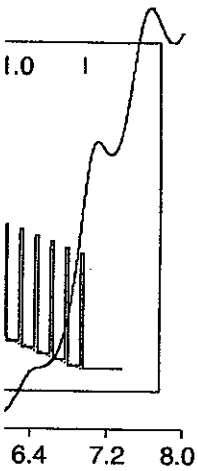

^{r} = 10) biased by a 2-V
ı probability spectrum.

and is to crowd more
riers. It is surprising,
N for N sufficiently
d by D and V, more
trum of a device with
he transmission pass
vice.
ı be altered by biasing
a potential difference
with a 2-V bias. That
tial is zero), while the
ative, the potential of
decrease of potential
arrier potential in the
ıe $2N + 1$ regions is
dpoint of the region.
d pulls them to lower
nsit this barrier from
erature), then we can
is device as a function
ıotonic function of V
complete discussion
elementary quantum

19

Variations on a Theme

The theme of this part of the book has been scattering, with an emphasis on tunneling through one or more barriers. We have seen that peaks in the transmission probability spectrum occur even in the classically forbidden regime. These peaks are due to resonances.

We now ask: What type of phenomena can be anticipated if we are able to fabricate two different types of barriers and place them adjacent to each other in any desired order? To study this problem we introduce two simple rectangular barriers A and B, shown in the inset of Fig. 19.1. We choose A to be a repelling barrier with energy 5.0 eV and width 1.0 Å surrounded on each side by regions of zero potential and width 2.0 Å each. Barrier B has a similar shape, with height 3.5 eV and width 2.0 Å, surrounded by two regions of width 3.0 Å at 0 eV.

In order to interpret the spectrum of the barrier AABB shown in Fig. 19.1, it is useful first to determine the principal features of the three building blocks AA, AB, and BB. The principal features of these spectra are the locations of the peaks. The energies of the peaks below 10 eV are collected in Table 19.1.

The peak at 4.7 eV consists of two overlapping resonances, one from the double barrier AA and one from the double barrier BB. This peak cannot be resolved by increasing the resolution of the scan.

To be more precise, the somewhat distorted peak at 4.7 eV, which consists of two overlapping peaks, cannot be resolved by probing with increased energy resolution, *subject to the boundary conditions specified:* $V_L = V_R = 0$. In computing transmission spectra for double and multiple potential barriers, we have observed that the lower energy peaks are narrower than the higher energy peaks. This suggests that we might be able to resolve the overlapping resonances buried in the peak at 4.7 eV

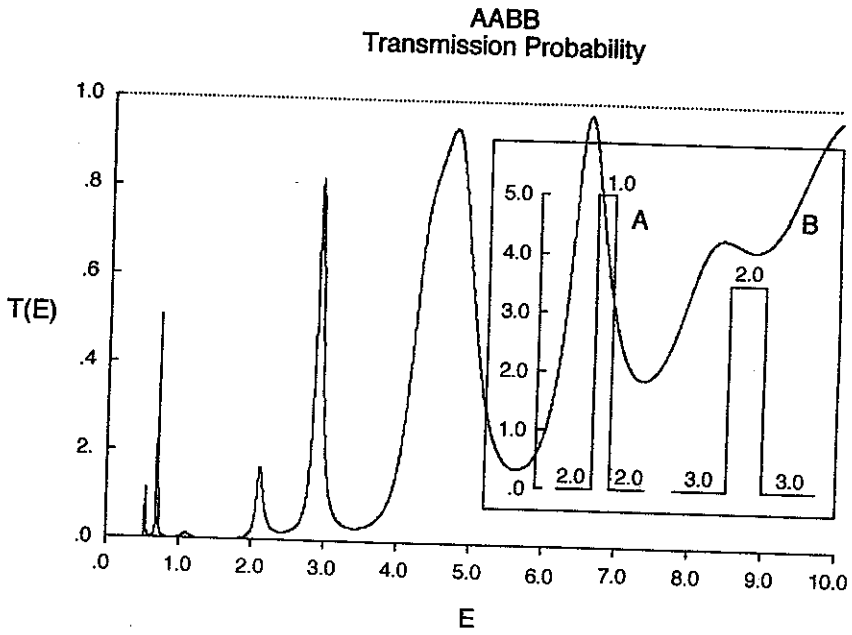

Fig. 19.1 Transmission probability for the multiple barrier AABB. The potentials A and B are shown in the inset. Each feature can be identified with a peak in one of the double barrier potentials AA, AB, or BB. The barriers AA and BB each contribute a peak in the range 4–5 eV. These peaks cannot be resolved by refining the energy scan.

by narrowing them. This can be done if we could somehow lower their energy. One possible way to do this would be to place this barrier inside a potential well with a depth of ~ 4 eV. To be more explicit, we could impose a potential on the asymptotic regions by setting $V_L = V_R = V$ and probe the target with an external low-energy electron beam with energy ϵ above the asymptotic limits V. This would probe the original potential (with $V_L = V_R = 0$) at the energy $E = V + \epsilon$.

The result of this kind of variable potential, low-energy spectroscopy is shown in Fig. 19.2 for $\epsilon = 0.1$ eV. The two peaks that overlap near 4.5 eV when $V_L = V_R = 0$ are narrow enough to be clearly resolved. They occur at $V = 4.0$ and 4.3 eV. We therefore expect the centers of these peaks occur at $E = 4.0$+0.1 and 4.3+0.1 eV in the original potential with $V_L = V_R = 0$. Further, these resonances can be unambiguously identified by computing (or probing) the probability distribution function for each at $V_L = V_R = V$, $E = V + \epsilon$.

It is gratifying to know that the individual components of an "unresolvable peak" can be unmasked by "pushing them down" to the energy of a low energy external electron probe beam by varying the boundary conditions.

In Table 19.2 we present the locations of peaks in the transmission probability spectrum $T(E)$ for various combinations of the potential barriers A and B. This includes degeneracies of unresolved/unresolvable peaks. This list does not include

Table 19.1 Energi
individual wells AA,

Energy of Pe
0.
0.
1.
2.
2.
4.
6.
8.

mirror image barrie
spectrum of a barr
symmetry of natur
Rather, it is the inv
specific, if the pot
the transmission pr
incident from the l

Problem Iden
Table 19.2.

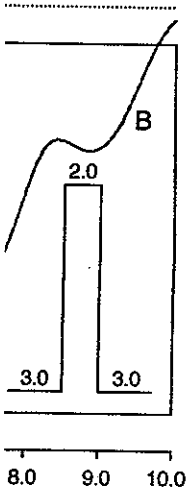

The potentials A and B
ıe of the double barrier
ı peak in the range 4–5

ver their energy. One
potential well with a
ial on the asymptotic
external low-energy
his would probe the
:.
ectroscopy is shown
4.5 eV when $V_L =$
at $V = 4.0$ and 4.3
4.0+0.1 and 4.3+0.1
ıese resonances can
)bability distribution

"unresolvable peak"
low energy external

ɜmission probability
:iers A and B. This
ist does not include

Table 19.1 Energies of peaks in the potential AABB, and source of the resonance in the individual wells AA, AB, and BB

Energy of Peak in AABB		Source of Resonance
0.5		BB
0.7		AB
1.1		AA
2.1		BB
2.9		AB
4.7	Unresolved doublet	AA,BB
6.5		AB
8.3		BB

mirror image barriers (BBA is the mirror image of ABB). The transmission probability spectrum of a barrier is identical to that of its mirror image. This has to do with a symmetry of nature. The symmetry is not a space reflection (or parity) symmetry. Rather, it is the invariance of the Hamiltonian (1.1) under time reversal. To be more specific, if the potential (Hamiltonian) that describes the system is time invariant, the transmission probability is the same whether the potential is probed by particles incident from the left or the right.

Problem. Identify the features in each of the transmission spectra presented in Table 19.2.

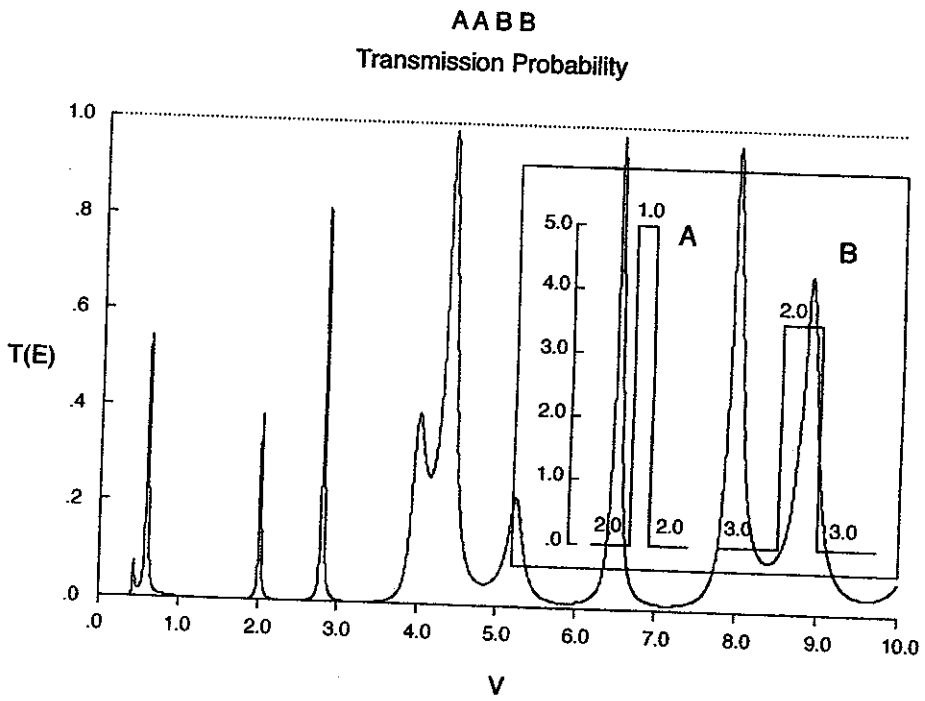

Fig. 19.2 Resolution of the "unresolvable" peaks between 4 and 5 eV in Fig. 19.1. The asymptotic left and right potentials are raised to a potential V, and the resulting potential is probed by an electron beam at energy ϵ (= 0.1 eV) above V. The transmission probability is probed as a function of $E = V + \epsilon$. The resolved peaks appear at $V = 4.0$, 4.3 eV, so are close to 4.1 and 4.4 eV in Fig. 19.1.

Table 19.2 Energie
for various combinatic

Barrier	Pea
AA	1.0,
AB	0.7,
BB	0.5,
AAA	(0.9
AAB	0.7,
ABA	(0.7
ABB	0.5,
BAB	(0.6
BBB	(0.5
AAAA	(0.8
AAAB	0.6.
AABA	0.7.
AABB	0.5
ABAB	(0.6
ABBA	0.5
BAAB	(0.6
ABBB	(0.5
BABB	0.5
BBBB	(0.5

Note: Some
[a] Multiplet u
[b] Multiplet re

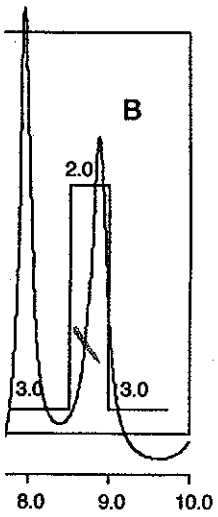

5 eV in Fig. 19.1. The
he resulting potential is
nsmission probability is
$V = 4.0$, 4.3 eV, so are

Table 19.2 Energies at which peaks occur in the transmission probability spectrum $T(E)$ for various combinations of the barriers A and B

Barrier	Peak Energies
AA	1.0, 4.1
AB	0.7, 2.9, 6.6
BB	0.5, 2.1, 4.7, 8.2
AAA	(0.9, 1.2), (3.8, 5.1), 9.3
AAB	0.7, 1.1, 2.9, 4.4, 6.7
ABA	(0.7, 0.8), (2.7, 3.2), (5.9, 7.4)
ABB	0.5, 0.8, 2.1, 2.9, 4.7, 6.5, 8.4
BAB	(0.6, 0.9), (2.6, 3.4), (6.0, 7.1)
BBB	(0.5, 0.6), (2.0, 2.4), (4.3, 5.1), (7.6, 8.9)
AAAA	(0.8, 1.0, 1.4), (3.5, 4.4, 5.5), 8.8
AAAB	0.6, 0.9, 1.3, 2.8, 3.9, 5.1, 6.7, 9.2
AABA	0.7, 0.8, 1.1, 2.6, 3.2, 4.4, 6.0, 7.4, 9.9
AABB	0.5, 0.7, 1.1, 2.1, 2.9, 4.7[a], 6.6, 8.4
ABAB	(0.6, 0.7, 0.9), (2.5, 2.9, 3.5), (5.7, 6.6, 7.7)
ABBA	0.5, 0.8[b], 2.1, 3.0[b], 4.7, 6.3, 6.8, 8.6
BAAB	(0.65, 0.75), 1.2, (2.7, 2.0), 4.5, 6.6, 9.9
ABBB	(0.5, 0.6), 0.8, (2.0, 2.3), 2.9, (4.3, 5.1), 6.5, (7.7, 9.0)
BABB	0.5, 0.6, 0.9, 2.1, 2.6, 3.4, 4.7, 6.0, 7.1, 8.4
BBBB	(0.50, 0.55, 0.62), (1.9, 2.2, 2.5), (4.1, 4.7, 5.3), (7.3, 8.2, 9.2)

Note: Some of the multiplets are grouped in parentheses.
[a] Multiplet unresolvable at any energy resolution.
[b] Multiplet resolvable at finer energy scan.